PCCP

ROYAL SOCIETY OF CHEMISTRY

PAPER

View Article Online
View Journal | View Issue

Cite this: *Phys. Chem. Chem. Phys.*, 2023, **25**, 31667

The effect of thionation of the carbonyl group on the photophysics of compact spiro rhodamine-naphthalimide electron donor–acceptor dyads: intersystem crossing, charge separation, and electron spin dynamics†

Xiao Xiao, ‡[a] Tong Mu, ‡[a] Andrey A. Sukhanov,‡[b] Yihang Zhou,[a] Peiran Yu,[a] Fabiao Yu,[c] Ayhan Elmali,[d] Jianzhang Zhao,*[a] Ahmet Karatay*[d] and Violeta K. Voronkova*[b]

Herein, a spiro rhodamine (**Rho**)-thionated naphthalimide (**NIS**) electron donor–acceptor orthogonal dyad (**Rho-NIS**) was prepared to study the formation of a long-lived charge separation (CS) state *via* the electron spin control approach. The transient absorption (TA) spectra of **Rho-NIS** indicated that the intersystem crossing (ISC) occurs within 7–42 ps to produce the ^{3}**NIS** state *via* the spin orbit coupling ISC (SOC-ISC). The energy order of ^{3}CS (2.01 eV in *n*-hexane, HEX) and ^{3}LE states (1.68 eV in HEX) depended on the solvent polarity. The ^{3}**NIS** state having n–π* character and a lifetime of 0.38 μs was observed for **Rho-NIS** in toluene (TOL). Alternatively, in acetonitrile (ACN), the long-lived ^{3}CS state (0.21 μs) with a high CS state quantum yield (Φ_{CS}, 97%) was produced with the ^{3}**NIS** state as the precursor and the CS took 134 ps. On the contrary, in the case of the reference **Rho**-naphthalimide (NI) **Rho-NI** dyad without thionation of its carbonyl group, a long-lived CS state (0.94 μs) with a high energy level (E_{CS} = 2.12 eV) was generated even in HEX with a lower Φ_{CS} (49%). In the presence of an acid, the **Rho** unit in the **Rho-NIS** adopted an open form (**Rho-o**) and the ^{3}**NIS** state was produced within 24–47 ps with the ^{1}**Rho-o** state as the precursor. Subsequently, slow intramolecular triplet–triplet energy transfer (TTET, 0.11–0.60 μs) produced the ^{3}**Rho-o** state (9.4–13.6 μs). According to the time-resolved electron paramagnetic resonance (TREPR) spectra of **NIS-NH$_2$**, the zero-field splitting (ZFS) parameter |*D*| and *E* of the triplet state were determined to be 6165 MHz and −1233 MHz, respectively, indicating that its triplet state has significant nπ* character, which was supported by its short triplet state lifetime (6.1 μs).

Received 9th October 2023,
Accepted 1st November 2023

DOI: 10.1039/d3cp04891h

rsc.li/pccp

Introduction

Charge separation (CS) is important in fundamental photochemistry studies,[1–15] as well as in photocatalysis,[4,6,16] photovoltaics,[17–20] photodynamic therapy,[21] thermally activated delayed fluorescence (TADF) emitters for application in OLEDs,[22–26] *etc.* One of the major goals in this area is to prolong the CS state lifetime, *i.e.*, to obtain a long-lived CS state, where the charge recombination (CR) should be thousands of time slower than the CS process.[2,3,27,28] The electron transfer in organic electron donor–acceptor dyads can be described by the Marcus equation:[29–31]

$$k_{ET} = \left(\frac{4\pi^3}{h^2\lambda k_B T}\right) V^2 \exp\left[-\frac{\left(\Delta G^0_{ET} + \lambda\right)^2}{4\lambda k_B T}\right] \quad (1)$$

In the equation, h and k_B represent the Planck and Boltzmann

[a] *State Key Laboratory of Fine Chemicals, Frontier Science Center for Smart Materials, School of Chemical Engineering, Dalian University of Technology, 2 Ling Gong Rd., Dalian 116024, P. R. China. E-mail: zhaojzh@dlut.edu.cn*
[b] *Zavoisky Physical-Technical Institute FRC Kazan Scientific Center of RAS, Sibirsky Tract 10/7, Kazan 420029, Russia. E-mail: vio@kfti.knc.ru*
[c] *Key Laboratory of Hainan Trauma and Disaster Rescue, The First Affiliated Hospital of Hainan Medical University, Hainan Medical University, Haikou 571199, P. R. China*
[d] *Department of Engineering Physics, Faculty of Engineering, Ankara University, 06100, Ankara, Turkey. E-mail: akaratay@eng.ankara.edu.tr*

† Electronic supplementary information (ESI) available: General experimental methods, synthesis of compounds, molecular structure characterization, computational details and additional spectra. CCDC 2294222 and 2294224. For ESI and crystallographic data in CIF or other electronic format see DOI: https://doi.org/10.1039/d3cp04891h

‡ These authors contributed equally to this work.

constants, respectively. ΔG^0_{ET} is the Gibbs free energy change of the electron transfer, λ is the total reorganization energy and V is the electronic matrix element. According to this equation, a few strategies have been developed to prolong the CS state lifetime. For example, reducing the electronic coupling matrix elements between the initial state and final state of the CS process, usually by introducing long and saturated linkers between the donor and acceptor. However, this method suffers from the drawback of challenging synthesis and slow charge transfer kinetics, which may be overcome by other relaxation processes of the ^{1}LE excited state (LE: locally excited), such as the direct decay of the S_1 state to the ground state (S_0). Alternatively, the Marcus inverted region effect was also exploited to prolong the CS state lifetime, although this effect is often less profound than theoretically predicted.

Recently, a new method to prolong the lifetime of the CS state was developed, *i.e.*, using the electron spin control effect.[3,28,32–36] The CS and CR processes are electron spin selective, *i.e.*, given that the CS has a singlet ^{1}LE precursor, the formation of the ^{1}CS state is dominant over the formation of the triplet ^{3}CS state, considering that the electron exchange energy (J) of the unpaired electrons is large.[3] Under this condition, the formation of the radical ion pair or the spin-correlated radical pair (SCRP) is unlikely.[37–39] Alternatively, an ^{3}LE precursor will dominantly give the ^{3}CS state, where the CR from the ^{3}CS state to the S_0 state is slower than the CR of the ^{1}CS state to produce the S_0 state because the $^3CS \rightarrow S_0$ process is electron spin forbidden. Thus, it is highly desirable to produce the ^{3}CS state rather than the ^{1}CS state. Therefore, efficient intersystem crossing (ISC) of the electron donor or acceptor will be beneficial for the formation of a long-lived ^{3}CS state.[3,11,40]

Concerning this, transition metal complexes have been used for the construction of electron donor–acceptor dyads to obtain the long-lived ^{3}CS state because the ISC in these metal complexes is fast and efficient, usually producing the ^{3}MLCT state (MLCT: metal-to-ligand-charge-transfer).[32,33,35,41–44] The fast ISC is due to the strong spin orbit coupling (SOC) effect of the transition metal ion. However, these precious metal complexes are expensive and the strong SOC may shorten the CS state lifetime.[35] Thus, heavy atom-free organic molecular systems showing efficient ISC are highly desirable for the preparation of electron donor–acceptor dyads to attain long-lived CS states by exploiting the spin control effect. However, this is challenging because very few heavy atom-free organic molecular systems show efficient ISC, and only limited examples of this approach have been reported.[3,45]

Recently, we used the spin–orbit charge transfer ISC (SOCT-ISC) for this purpose,[40] which requires an orthogonal geometry between the donor and acceptor units in the molecular structure of the dyad.[5,46–48] However, the ISC is slow for our previously reported dyad.[11,40] Thus, it is clear that more methods for the formation of the ^{3}CS state *via* the electron spin control effect should be studied. We noted that the thionation of the carbonyl group of a chromophore may induce efficient ISC in the otherwise strongly fluorescent chromophores.[49–55] In this case, the molecular derivatization involves the replacement of only one atom. Another advantage of thionation is the enhanced electron-accepting ability of the resulting thionated chromophore.[56] Inspired by the previously reported spiro donor–acceptor dyad based on a rhodamine (**Rho**) and naphthalimide (NI) dyad molecular structure to obtain the long-lived ^{3}CS state *via* the electron spin control method and to enhance the ISC to populated the ^{3}LE state,[40] herein we performed further derivatization, *i.e.*, thionation of the NI unit, to enhance the ISC ability and the electron-accepting ability of the NI unit (**Rho-NIS**, Scheme 1). The electron transfer and ISC processes of the compounds were studied *via* steady state

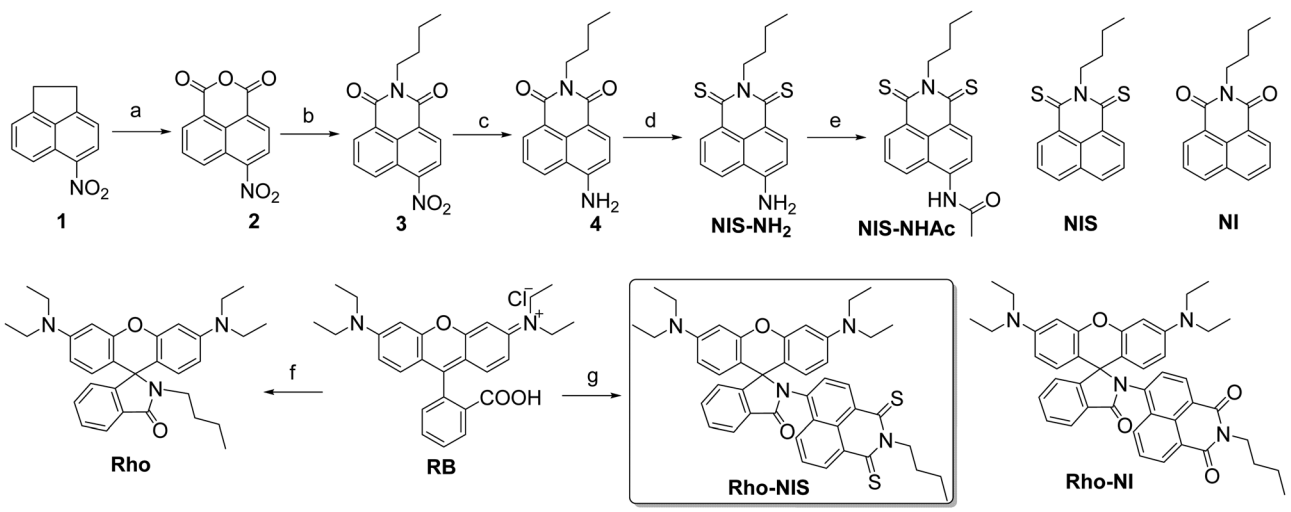

Scheme 1 Molecular structures of rhodamine-thionated naphthalimide derivatives. (a) $Na_2Cr_2O_7{\cdot}2H_2O$, AcOH, N_2, reflux, 5 h, and yield: 55%. (b) *n*-butylamine, EtOH, N_2, reflux, 2 h, and yield: 54%. (c) $SnCl_2{\cdot}2H_2O$, Con. HCl, EtOH, N_2, RT, 15 min, and yield: 81%. (d) Lawesson's reagent, dry toluene, N_2, reflux, 21 h, and yield: 28%. (e) Acetic anhydride, acetic acid, 130 °C, 5 h; and yield: 26%. (f) $POCl_3$, dry dichloromethane (DCM), reflux, 5 h; *n*-butylamine, dry acetonitrile (ACN), Et_3N, reflux, 25 h; and yield: 42%. (g) $POCl_3$, dry DCM, reflux, 5 h; **NIS-NH$_2$**, dry ACN, Et_3N, reflux, 25 h; and yield: 50%.

UV-vis absorption and fluorescence spectroscopy, femtosecond and nanosecond transient absorption spectroscopic methods, timed-resolved electron paramagnetic resonance (TREPR) spectroscopy, and theoretical computations.

Experimental

General method

All chemicals used in the synthesis were analytically pure. The solvents for the synthesis were dried before use. UV-vis spectra were recorded using a UV-2550 spectrophotometer (Shimadzu Ltd, Japan). Fluorescence emission spectra were recorded using an FS5 spectrofluorometer (Edinburgh Instruments Ltd, UK). Fluorescence lifetimes were recorded using an OB920 luminescence lifetime spectrometer (Edinburgh Instrument Ltd, UK), and a picosecond EPL laser was used for excitation. Fluorescence quantum yields (Φ_F) were measured using an absolute photoluminescence quantum yield spectrometer (Quantaurus-QY Plus C13534-11, Hamamatsu Ltd, Japan).

Synthesis of Rho-NIS

Under an N_2 atmosphere, rhodamine B (160.0 mg, 0.33 mmol) was dissolved in dry dichloromethane (DCM, 5 mL), and then $POCl_3$ (0.2 mL) was added dropwise. The mixture was refluxed and stirred for 5 h. The solvent was evaporated under reduced pressure, and then the crude product was dissolved in dry CH_3CN (8 mL). The mixture was added dropwise to a solution of compound **NIS-NH$_2$** (60.1 mg, 0.20 mmol) and Et_3N (0.4 mL) in CH_3CN (7 mL), and then the mixture was refluxed and stirred for 22 h. After the reaction was finished, the solvent was evaporated under reduced pressure, and the crude product was purified by column chromatography (silica gel, DCM) to give the product as a brown solid (72.4 mg, yield: 50%). M.p.: 227.6–228.8 °C. ^{1}H NMR ($CDCl_3$, 400 MHz): δ 8.75 (d, J = 7.5 Hz, 1H), 8.59 (d, J = 8.3 Hz, 1H), 8.08 (d, J = 7.4 Hz, 1H), 7.73–7.61 (m, 3H), 7.35–7.27 (m, 2H), 6.72–6.68 (m, 2H), 648–6.42 (m, 2H), 6.26–6.20 (m, 2H), 5.93 (s, 1H), 5.30–5.25 (m, 2H), 3.42–3.36 (m, 4H), 3.19–3.15 (m, 4H), 1.89–1.82 (m, 2H), 1.47–1.41 (m, 2H), 1.21 (t, J = 7.0 Hz, 6H), 1.03–0.96 (m, 9H). ^{13}C NMR ($CDCl_3$, 125 MHz): δ 191.01, 190.61, 166.93, 154.27, 153.60, 151.63, 149.29, 148.92, 137.92, 137.48, 133.31, 131.86, 130.57, 129.49, 129.32, 129.07, 128.75, 127.61, 126.65, 124.63, 124.13, 123.78, 108.39, 107.59, 106.51, 105.69, 97.84, 97.61, 54.87, 44.49, 44.32, 31.94, 31.60, 29.67, 27.35, 22.66, 20.02, 14.13, 13.76, 12.55, 12.39. HRMS-ESI ($[C_{44}H_{44}N_4O_2S_2 + H]^+$), m/z: calcd: 725.2984; found: 725.2961.

Single crystal X-ray diffraction

Single crystals of **Rho-NIS** and **NIS-NHAc** were obtained *via* the slow diffusion of a layer of *n*-hexane (HEX) into the DCM solution of the compounds. The X-ray diffraction data of the single crystals were measured and collected on a Bruker D8 Venture CMOS-based diffractometer with graphite monochromatized Mo Kα radiation (λ = 0.71073 Å) at 120 K, using the SMART and SAINT programs. The X-ray diffraction data were analyzed with the ShelXT structure solution program using Intrinsic Phasing and refined with the ShelXL refinement package using least squares minimization implemented in Olex2.[57] CCDC numbers are 2294224 (**Rho-NIS**) and 2294222 (**NIS-NHAc**), respectively.†

Electrochemical studies

Cyclic voltammetry curves were recorded using a CHI610D electrochemical workstation (CHI instruments, Inc., Shanghai, China). A platinum electrode was used as the counter electrode and a glassy carbon electrode as the working electrode. The ferrocenium/ferrocene (Fc^+/Fc) redox couple was used as the internal reference. Spectroelectrochemistry was performed using a 0.1 cm path length quartz electrochemical cell. Gauze platinum acted as the working electrode and platinum wire as the counter electrode. The potential was regulated using a CHI610D electrochemical workstation and the spectra were recorded using an Agilent 8453 UV-vis spectroscopy system (Agilent Technologies Inc., USA). In both cases, $Bu_4N[PF_6]$ was used as the supporting electrolyte and the $Ag/AgNO_3$ (0.1 M in ACN) couple was used as the reference electrode. The samples were deaerated with N_2 for *ca.* 15 min before measurement, and the N_2 atmosphere was maintained during the measurement.

Nanosecond transient absorption spectroscopy

Nanosecond transient absorption spectra were studied using an LP980 laser flash photolysis spectrometer (Edinburgh Instruments Ltd, UK), and the signal was digitized with a Tektronix TDS 3012B oscilloscope. The collinear configuration of the pump and probe beams was used for the measurements. The sample solutions were purged with N_2 for 15 min before measurement and excited with a nanosecond pulsed laser (OpoletteTM 355II + UV nanosecond pulsed laser. OPOTEK, USA). The typical laser power was 5 mJ per pulse. The data were analyzed using L900 software.

Femtosecond transient absorption spectroscopy

The fs-TA experiments were performed using a Ti:sapphire laser system with an ~100 fs pulse duration and 1 kHz repetition rate (Astrella, Coherent) and a commercial ultrafast transient absorption spectrometer (Ultrafast System, Helios). The excitation wavelength was determined from the steady-state UV-vis absorption spectra and generated in an optical parametric amplifier (TOPAS, Light Conversion). The magic angle between the probe and the pump beam polarization direction was used. The Surface Xplorer and Glotaran software were used for processing the experimental data based on the data after chirp correction.[58,59]

Time-resolved electron paramagnetic resonance spectra

Samples were studied in a frozen solution of TOL/2-methyltetrahydrofuran (2-MeTHF, 1/1, v/v) with a concentration of 1×10^{-4} M and transferred to quartz tubes (outer diameter: 4.5 mm and inner diameter: 3.0 mm). The time-resolved continuous-wave (CW) EPR measurements were performed on an X-band and Q-band EPR Elexsys E-580 spectrometer (Bruker) with a

dielectric ring X-Band ER 4118X-MD5-W1 resonator at a temperature of 80 K. The oxygen was removed with five freeze–pump–thaw cycles. Optical excitation was carried out using an Nd:YAG pulse laser (LQ629 Solar LS) at a wavelength of 355 nm with a pulse energy of 1 mJ and frequency of 100 Hz. The spectra were simulated using the EasySpin package based on Matlab.[60]

DFT calculations

The geometries of the compounds were optimized using density functional theory (DFT) with the B3LYP functional and 6-31G(d) basis set. The spin density surfaces at the optimized triplet state geometries were visualized. There were no imaginary frequencies for all optimized structures. The triplet excited state energy of the compounds was calculated by time-dependent DFT (TDDFT) with the B3LYP functional and 6-31G(d) basis set based on the optimized ground-state geometry. Natural transition orbital (NTO) analysis was performed using the Multiwfn program.[61] All calculations were performed using Gaussian 09.[62]

Results and discussion

Molecular structure design rationale

Previously, we studied a spiro electron donor–acceptor dyad based on rhodamine and NI units to realize the long-lived ^{3}CS state *via* electron spin control, which was achieved by the SOCT-ISC mechanism to produce the ^{3}LE precursor in the CS process.[40] However, the ISC of this heavy atom-free dyad is slow (^{1}CS → ^{3}NI takes *ca.* 8 ns), which is not beneficial for efficient secondary CS to obtain the long-lived ^{3}CS state. Thus, to improve the ISC kinetics, and consequently the CS yield, herein we performed the thionation reaction of the carbonyl group of the NI electron acceptor in the dyad to prepare a new dyad (**Rho-NIS**, Scheme 1). The advantage of this one-atom replacement derivatization includes a red-shifted absorption,[51] increased electron-accepting ability,[56] and accelerated ISC process. Previously, it was reported that a thionyl carbonyl-containing chromophore showed ultrafast ISC (0.6 ps).[49,63] The perturbation in the molecular structure is negligible because only two atoms of the previously reported dyads are replaced (Scheme 1). The compounds **NIS** and **NIS-NH$_2$** were used in this study as reference compounds (Scheme 1). The synthesis of the compounds is based on the routine derivatization methods of rhodamine and NI chromophores,[40,64] the yields were satisfactory, and the molecular structures were fully characterized (see Experimental).

The molecular structures of **Rho-NIS** and **NIS-NHAc** were determined by single-crystal X-ray diffraction (Fig. 1). Each unit cell of **Rho-NIS** and **NIS-NHAc** contains four molecules and has a triclinic crystal structure. X-ray diffraction showed that the centroid-to-centroid distance between xanthene and the **NIS** units in **Rho-NIS** is 5.3 Å and the dihedral angle between the xanthene and **NIS** units is 53.0° (Fig. 1). In the case of the previously reported **Rho-NI** dyad, the dihedral angle between

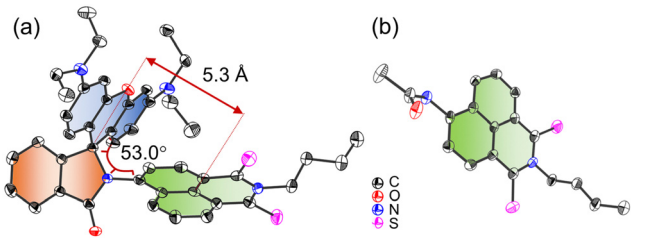

Fig. 1 The ORTEP view of the molecular structures of (a) **Rho-NIS** and (b) **NIS-NHAc** determined by single-crystal X-ray diffraction (50% probability thermal ellipsoids). Hydrogen atoms are omitted for clarity.

xanthene and the NI moiety was 70.8°.[40] The xanthene moiety adopts a planar geometry, which was the same as observed for **Rho-NIS** (Fig. 1a). We also obtained a single crystal of the reference compound **NIS-NHAc** (Fig. 1b), where its C=S bond length is 1.64 Å, which is close to that in **Rho-NIS** (1.64 Å). Moreover, the C–N bond length at the 4-position of NI in **NIS-NHAc** is 1.42 Å, while that in **Rho-NIS** is 1.43 Å. It should be noted that the C=S bond length is longer than the corresponding C=O bond length (1.24 Å),[40] and the C–N bond length at the linkage between xanthene and the NI moiety is 1.43 Å.[40] These results show that the perturbation of the sulfur substitution has a negligible impact on the geometry of the dyad.

Steady-state UV-vis absorption and luminescence spectra

The UV-vis absorption of the compounds was studied (Fig. 2a). **NIS** showed an absorption band centered at 438 nm, which is redshifted by 110 nm compared to that of the native NI chromophore.[65–67] In the case of **NIS-NH$_2$**, a further red shift to 526 nm was observed, which is due to the attachment of the amino group at the 4-position of the NI moiety.[51] Interestingly, **Rho-NIS** showed a major absorption band centered at 453 nm, which is very close to that of **NIS**. This result was rationalized by the acetylation of the amino group and the restricted conformation, which reduced the electron-donating ability and π-conjugation of the lone electron pairs on the N atom with the NI chromophore.[68,69] It should be noted that the previously reported analogue (**Rho-NI**, without thionation of the carbonyl group) showed absorption in the range of $<$400 nm,[40] whereas that of **Rho-NIS** was $>$400 nm, which is beneficial for harvesting visible light.

Rhodamine is known to have two structures, *i.e.*, opened and closed structures, and the transformation between these two structures can be realized in the presence of acid and base.[70–75] Interestingly, the attachment of the **NIS** moiety to the rhodamine chromophore does not change the opening and closing reversible transformation of the rhodamine moiety in the presence of acid and base (Fig. 2b and c, respectively). In the presence of trifluoroacetic acid (TFA), the **Rho** unit in **Rho-NIS** transforms from the closed form to the opening form, and accordingly a strong, broad absorption in the visible spectral region of 500–650 nm was observed (Fig. 2b). The absorption band of the open form of **Rho** disappeared with the addition of a base such as triethylamine (TEA) (Fig. 2c). This property may

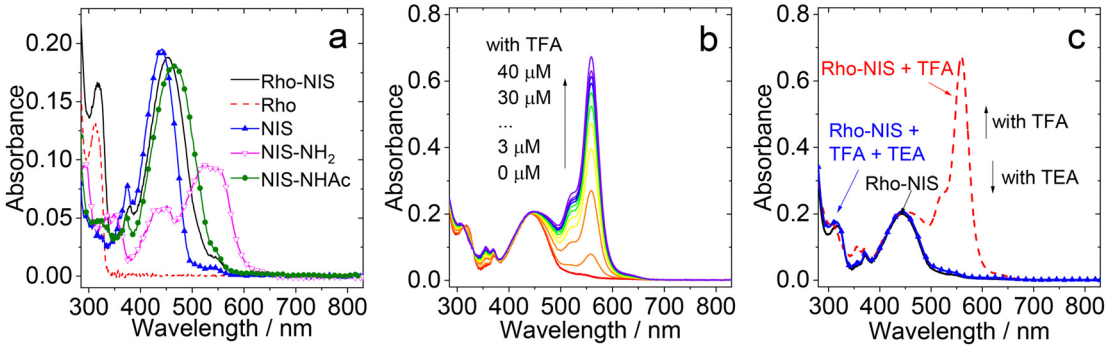

Fig. 2 (a) UV-vis absorption spectra of the compounds in TOL. (b) The evolution of the UV-vis absorption spectra of **Rho-NIS** with the incremental addition of trifluoroacetic acid (TFA) and (c) with the addition of TFA (c = 40 μM) or triethylamine (TEA, neat, 10 μL) in MeOH. c = 1.0 × 10^{-5} M. 25 °C.

endow the compound with additional functionality, such as acid-activated PDT capability. Moreover, the evolution of the UV-vis absorption spectra of **Rho-NIS** upon the ring-opening reaction indicated that the blue-shifted absorption of the **NIS-NH_2** unit in **Rho-NIS** is mainly due to the acetylation reaction, not the sterically encumbered microenvironment of the N atom connected to the spiro C atom. This is because for **Rho-NIS** with the **Rho** unit in the open form (no conformation restriction), the absorption band centered at 453 nm did not change to 526 nm (that of **NIS-NH_2**).

Fig. 3a shows that the fluorescence of the closed-ring structure of the **Rho** unit is quenched in **Rho-NIS**, where the possible reason for this is electron transfer or Förster resonance energy transfer (FRET) to the **NIS** moiety. Based on the femtosecond transient absorption (fs-TA) spectral studies (see later section), charge transfer from **Rho** to **NIS** was not observed in TOL upon photoexcitation. Therefore, FRET is the most probable reason for the fluorescence quenching of the closed ring structure of **Rho**. Fig. 3b shows that the fluorescence of **NIS-NH_2** (Φ_F = 0.8%) was quenched in **Rho-NIS** (Φ_F = 0.3%), and we attribute this quenching to the acetylation of the amino group in **Rho-NIS**, which was also proven by the weaker fluorescence of the reference compound **NIS-NHAc** (Φ_F = 0.2%).

In the case of **Rho-NIS**, in the presence of trifluoroacetic acid (TFA), the fluorescence was enhanced and peaked at 583 nm (Fig. 3c), which is attributed to the **Rho** moiety in the open form. Interestingly, the fluorescence of **Rho-NIS** (Φ_F = 0.5%, Table 1) was quenched compared to **Rho** under the same condition (Φ_F = 44.2%, Fig. 3d). This is probably due to the charge transfer from the **Rho** moiety in the open form to the **NIS** moiety. In this case, no FRET to the **NIS** moiety occurs. The fluorescence decay trace at 583 nm of **Rho-NIS** under this condition has a biexponential feature and the lifetime is 0.64 ns (population rate: 70%)/2.3 ns (30%) (Fig. S17, ESI†). The component with the lifetime of 2.3 ns is attributed to the open form of the **Rho** moiety in **Rho-NIS**, which is the same with that of **Rho** with the addition of TFA, showing mono-exponential decay with the lifetime of 2.3 ns (Fig. S17, ESI†). The short-lived component with the lifetime of 0.64 ns further indicates that there is a non-radiative transition process from the singlet state of the **Rho** moiety in the open form.

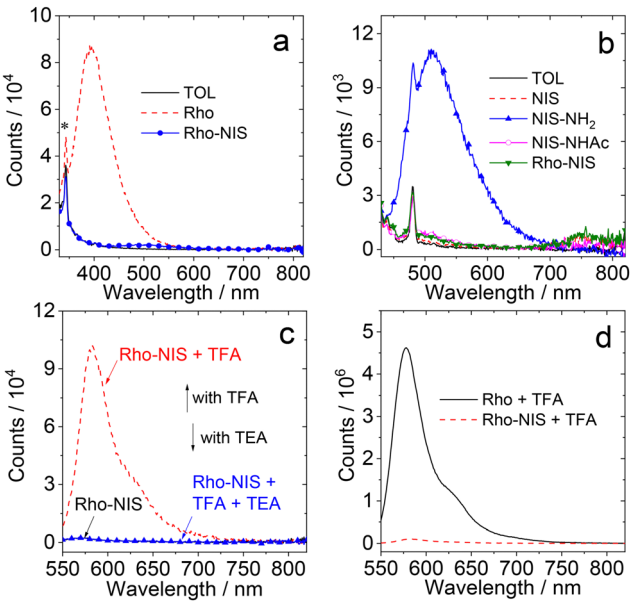

Fig. 3 Fluorescence emission spectra of the compounds in TOL. (a) λ_{ex} = 310 nm and (b) λ_{ex} = 420 nm. Optically matched solutions were used (all solutions show the same absorbance at the excitation wavelength, A_{ex} = 0.1). Asterisks in (a) and (b) stand for the Raman scattering peak of the solvent. (c) Fluorescence emission spectra of **Rho-NIS** with the addition of TFA (c = 40 μM) or TEA (neat, 10 μL) in MeOH. (d) The comparison of fluorescence emission spectra of **Rho** and **Rho-NIS** with the addition of TFA (c = 40 μM) in MeOH. λ_{ex} = 540 nm. c = 1.0 × 10^{-5} M. 25 °C.

To determine the energy of the ^{3}**NIS** state of the compounds, their phosphorescence emission spectra in frozen 2-methyltetrahydrofuran (2-MeTHF) at 77 K were studied (Fig. S18, ESI†). The phosphorescence emission bands were observed in the range of 700–825 nm under these conditions. Based on the similar spectra observed for **NIS** and **Rho-NIS**, the phosphorescence bands are attributed to the ^{3}**NIS** state. According to the on-set of the phosphorescence band on the high-energy side (can be approximated as the vibrational 00 transition of $T_1 \rightarrow S_0$ radiative relaxation), the ^{3}**NIS** state energy was approximated to be 1.71 eV for **NIS** and 1.68 eV for **Rho-NIS** (Table 1). These values are close to the ^{3}**NIS** state energy (1.65 eV) calculated using the ZINDO/S semiempirical quantum

Table 1 Photophysical properties of the compounds[a]

Compounds	λ_{abs}[b]	ε[c]	λ_F[d]	Φ_F[e]	τ_F[f]	Φ_Δ[g]	λ_P[h]	τ_P[i]
NIS	438	1.94	—[j]	0.4	—[j]	0.46; 0.04[k]	725	1.6 ms
NIS-NH$_2$	526	0.96	506	0.8	8.4 ns	0.95; 0.58[k]	—[j]	—[j]
NIS-NHAc	463	1.80	494	0.2	4.8 ns	1.0; 0.46[k]	—[l]	—[l]
Rho	313	1.32	391	1.1	1.7 ns (73%) 4.7 ns (27%)	0.27; 0[k]	—[j]	—[j]
Rho + TFA[k]	557[m]	6.01[m]	578	44.2	2.3 ns	—[j]	—[j]	—[j]
Rho-NIS	453	1.88	495	0.3	—[j]	0.72; 0[k]	740	7.0 μs (89%) 16.2 μs (11%)
Rho-NIS + TFA[k]	559	6.73	583	0.5	0.64 ns (70%) 2.3 ns (30%)	0.87[n] 0.43[o]	—[l]	—[l]

[a] In TOL. [b] Maximal UV-vis absorption wavelength. $c = 1.0 \times 10^{-5}$ M in nm. [c] Molar absorption coefficient, in 10^4 M^{-1} cm^{-1}. [d] Maximal fluorescence emission wavelength in nm. [e] Fluorescence quantum yields in %. [f] Fluorescence lifetime. $c = 1.0 \times 10^{-5}$ M in ns. [g] Singlet oxygen quantum yields. [h] Maximum phosphorescence emission wavelength in MeTHF in nm at 77 K. [i] Phosphorescence lifetimes (λ_{ex} = 445 nm), $c = 1.0 \times 10^{-4}$ M, 77 K. [j] Not observed. [k] In MeOH. [l] Not measured. [m] Literatures values, ref. 76. [n] λ_{ex} = 430 nm. [o] λ_{ex} = 560 nm.

chemical method and slightly higher than that estimated by DFT calculation (1.57 eV).[51,77]

As an approximation of the ISC efficiency, the singlet oxygen quantum yields (Φ_Δ) of the compounds were measured (Table 1). In the case of **NIS**, the Φ_Δ in TOL and MeOH are 46% and 4%, respectively, which are close to the reported Φ_Δ of **NIS** in TOL (32%).[51] Interestingly, the reported **NIS** analogue, thionated perinone with a single thionated carbonyl group, has the Φ_Δ of 100%.[52] **NIS-NH$_2$** has higher Φ_Δ (95% in TOL and 58% in MeOH) compared to **NIS**. We propose that although the ISC quantum yields in all these thionated compounds may be close to unity, the singlet oxygen quantum yields are dependent on the triplet state lifetime of the compounds (see later section). A short triplet state lifetime may reduce the singlet oxygen quantum yield, although for **Rho-NIS**, Φ_Δ is 72% in TOL and no singlet oxygen photosensitizing was observed in MeOH upon excitation at the **NIS** moiety (λ_{ex} = 430 nm). In the presence of acid, the Φ_Δ of **Rho-NIS** in MeOH increased to 87% upon excitation at the **NIS** moiety (430 nm). Also, the Φ_Δ was 43% upon excitation at the rhodamine moiety in the open form (560 nm). In the case of **Rho** in the open form, no singlet oxygen photosensitizing was observed.

Electrochemistry study

To calculate the Gibbs free energy changes (ΔG^0_{CS}) in the photo-induced CS and determine the energy of the CS states, the redox potentials of the compounds were studied *via* cyclovoltammetry (Fig. 4a and b). In the case of the **Rho** reference compound, two reversible oxidation waves were observed at +0.51 V and +0.64 V (*vs.* Fc/Fc$^+$), respectively. No reduction wave was observed in the potential range applied in this study. Alternatively, in the case of **NIS**, one reversible reduction wave was observed at −1.09 V, and this wave was anodically shifted by 0.66 V compared to the native NI (unthionated, −1.75 V). This result indicates that **NIS** is a stronger electron acceptor than the un-thionated NI. With the attachment of the amino substituent, **NIS-NH$_2$** showed a cathodically shifted reduction wave at −1.29 V, indicating that **NIS-NH$_2$** is a poorer electron acceptor than **NIS**. This is reasonable because that the –NH$_2$ in **NIS-NH$_2$** is an electron-donating group. In the case of **Rho-NIS**,

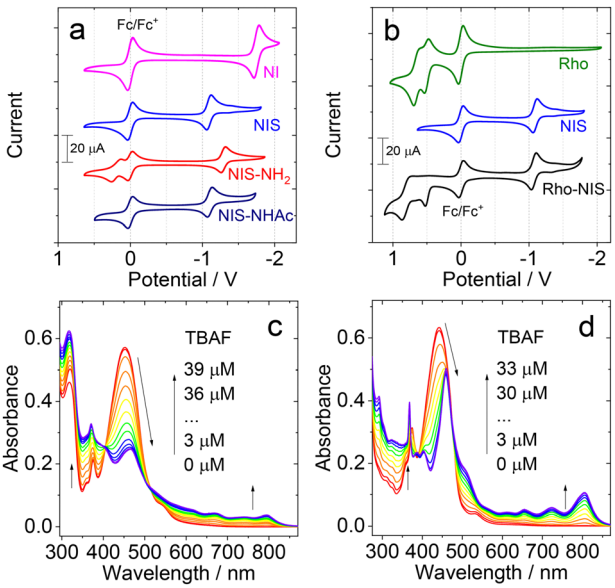

Fig. 4 (a) and (b) Cyclic voltammograms of the compounds in deaerated ACN. Ferrocene (Fc/Fc$^+$) was used as the internal reference (set as 0 V in the cyclic voltammograms). 0.10 M $Bu_4N[PF_6]$ as the supporting electrolyte and Ag/$AgNO_3$ as the reference electrode. Scan rate: 100 mV s^{-1}. $c = 1.0 \times 10^{-3}$ M. UV-vis absorption spectra of (c) **Rho-NIS** and (d) **NIS** chemically reduced with tetrabutylammonium fluoride (TBAF) to generate **NIS**$^{\bullet-}$ in deaerated DMF. $c = 3.0 \times 10^{-5}$ M. 25 °C.

two irreversible oxidation waves were observed at +0.52 V and +0.87 V, as well as a pseudo reversible reduction wave at −1.07 V. It should be noted that the amino**NIS** moiety in **Rho-NIS** is similar to **NIS**, not **NIS-NH$_2$**. This result is in agreement with the UV-vis absorption spectral studies.

Based on the electrochemical data, the driving force for the photo-induced CS, *i.e.* ΔG^0_{CS}, was calculated using the Rehm–Weller equation (eqn (S2)–(S5), refer to the ESI,† for details), as follows:[78–80]

$$\Delta G^0_{CS} = e[E_{OX} - E_{RED}] - E_{00} + \Delta G_S \quad (2)$$

$$\Delta G_S = -\frac{e^2}{4\pi\varepsilon_S\varepsilon_0 R_{CC}} - \frac{e^2}{8\pi\varepsilon_0}\left(\frac{1}{R_D} + \frac{1}{R_A}\right)\left(\frac{1}{\varepsilon_{REF}} + \frac{1}{\varepsilon_S}\right) \quad (3)$$

Table 2 Electrochemical redox potentials, Gibbs free energy changes of the charge separation (ΔG^0_{CS}) and the energy of the charge-separated state (E_{CSS}) of the compounds in different solvents[a]

			ΔG^0_{CS} (eV)/E_{CSS} (eV)			
	E_{OX} (V)	E_{RED} (V)	HEX	TOL	THF	ACN
Rho	+0.51, +0.64	—[b]	—[c]	—[c]	—[c]	—[c]
NI	—[b]	−1.75	—[c]	—[c]	—[c]	—[c]
NIS	—[b]	−1.09	—[c]	—[c]	—[c]	—[c]
NIS-NH$_2$	+0.19	−1.29	—[c]	—[c]	—[c]	—[c]
NIS-NHAc	—[b]	−1.10	—[c]	—[c]	—[c]	—[c]
Rho-NIS	+0.52, +0.87	−1.07	0.33/2.01	0.22/1.90	−0.05/1.63	−0.16/1.52

[a] Cyclic voltammetry in N_2-saturated solvent containing 0.10 M $Bu_4N[PF_6]$. Pt electrode as the counter electrode, glassy carbon as the electrode working electrode, ferrocene (Fc/Fc^+) as the internal reference (set as 0 V in the cyclic voltammograms), and $Ag/AgNO_3$ couple as the reference electrode. In ACN. E_{00} = 1.68 eV. E_{00} is the T_1 state energy of **NIS** estimated by 00 transition based on phosphorescence emission spectra. THF stands for tetrahydrofuran. [b] Not observed. [c] Not applicable.

$$\Delta G^0_{CR} = -(\Delta G^0_{CS} - E_{00}) \quad (4)$$

$$E_{CSS} = e[E_{OX} - E_{RED}] + \Delta G_S \quad (5)$$

The data showed that CS may occur for **Rho-NIS** upon photoexcitation in a polar solvent, such as ACN (Table 2). However, this does not mean that the CS state will be observed experimentally because the lowest state must be a CS state not ^{3}LE state, and the CS process must outcompete the other relaxation processes of the ^{1}LE state. The ^{3}**NIS** state energy of **Rho-NIS** was estimated by 00 transition of the phosphorescence emission spectra and determined to be 1.68 eV.[51] It should be noted this value is much lower than that of the native NI chromophore (2.25 eV).[81] The calculation showed that the energy of the CS state (2.01 eV in HEX and 1.90 eV in TOL) is higher than the ^{3}**NIS** state (Table 2) in non-polar and low-polar solvents. In polar solvents such as ACN, the energy of the CS state (1.52 eV) was lower than the ^{3}**NIS** state (1.68 eV). It should be noted that the ^{3}LE state energy level was not significantly affected by a variation in the solvent polarity.

Furthermore, to facilitate the assignment of the CS state in the transient absorption spectra, chemical reduction of the compounds was performed to obtain the UV-vis absorption of their anion (Fig. 4c and d). In the case of **Rho-NIS**, upon reduction with tetrabutylammonium fluoride (TBAF), the absorption band centered at 453 nm decreased, and a new dominant absorption band centered at 462 nm and weaker bands centered at 668 nm and 794 nm developed, which are attributed to the **NIS**$^{\bullet-}$ radical anion species (Fig. 4c). Similar results were observed for the reference compound **NIS** (Fig. 4d). The UV-vis spectra of **NIS**$^{\bullet-}$ for **NIS** were also computed by the TDDFT method (Fig. S52, ESI†), which supports the experimental results. With the addition of TBAF, **NIS-NH$_2$** showed absorption bands centered at 390 nm and 600 nm (Fig. S19, ESI†), which are attributed to [**NIS-NH$_2$**]$^{\bullet-}$ and different from the **NIS**$^{\bullet-}$ of **NIS** and **Rho-NIS**. These results are in agreement with the UV-vis absorption spectral studies and further indicate that the acetylation of the amino group and the conformation restriction of **Rho-NIS** reduced the electron-donating ability of the N atom and the π-conjugation of the lone electron pairs on the N atom with the NI chromophore. The absorption of the NI radical anion (NI$^{\bullet-}$) without thionation of the carbonyl group was observed at 420 nm, 491 nm and 830 nm, which is different from that of the **NIS**$^{\bullet-}$ of **NIS** and **Rho-NIS**.[82–84]

Femtosecond transient absorption (fs-TA) spectra

To study the excited-state dynamics of the compounds upon photoexcitation, the fs-TA spectra of the dyads were recorded in solvents with different polarity (Fig. 5). The data (Fig. 5a–c) were analyzed with singular value decomposition (SVD) and global analysis using a linear unidirectional decay scheme. The evolution-associated difference spectra (EADS) for each kinetic constant were obtained by global analysis (Fig. 5d–f). In the case of **NIS**, the fs-TA spectra in TOL are shown in Fig. 5c. Also, the result of a target analysis of the fs-TA data with a sequential model was obtained (Fig. 5f). The ground-state bleaching (GSB) band was observed in the range of 420–500 nm, which is in agreement with the steady-state absorption spectrum (Fig. 2). The S_1 state with an absorption band centered at 505 nm and 740 nm was populated after photoexcitation. Then, the ^{3}**NIS** state with the absorption at 510 nm was generated by the fast ISC process within 10.6 ps from the ^{1}**NIS** state, which was attributed to the spin orbit coupling ISC (SOC-ISC) mechanism. Similar results were observed for **NIS** in ACN with the ISC process of 1.4 ps (Fig. S20, ESI†). It should be noted that the first species with the lifetime of 277 fs in Fig. 5f is the signal of the TOL solvent, which cannot be neglected in the global fitting. A similar result was observed in Fig. 5d. The ^{3}**NIS** state did not decay completely within the available time window of the fs-TA spectrometer, which is supported by the ns-TA spectra (see later section). In the case of **NIS-NH$_2$**, its ESA bands were different from that of **NIS**, and the ISC from ^{1}**NIS-NH$_2$** → ^{3}**NIS-NH$_2$** takes 31 ps (Fig. S21, ESI†). Thus, the ISC kinetics is in good agreement with the theoretically predicted ISC rate constants of ∼10 ps.[85] Interestingly, the ISC kinetics of **NIS** is similar to that of the unsubstituted NI (∼10–20 ps).[86] It should be noted for the 4-amino-substituted NI, the ISC is negligible.[66,87,88] The ISC kinetics of the thionated NI is similar to that observed for the thionated perylene bisimide (PBI).[49,63]

The fs-TA spectra of **Rho-NIS** in different solvents upon excitation are shown in Fig. 5a and b, together with the EADS obtained from global analysis. In TOL, two species were required for the satisfactory fitting of the spectra (independent

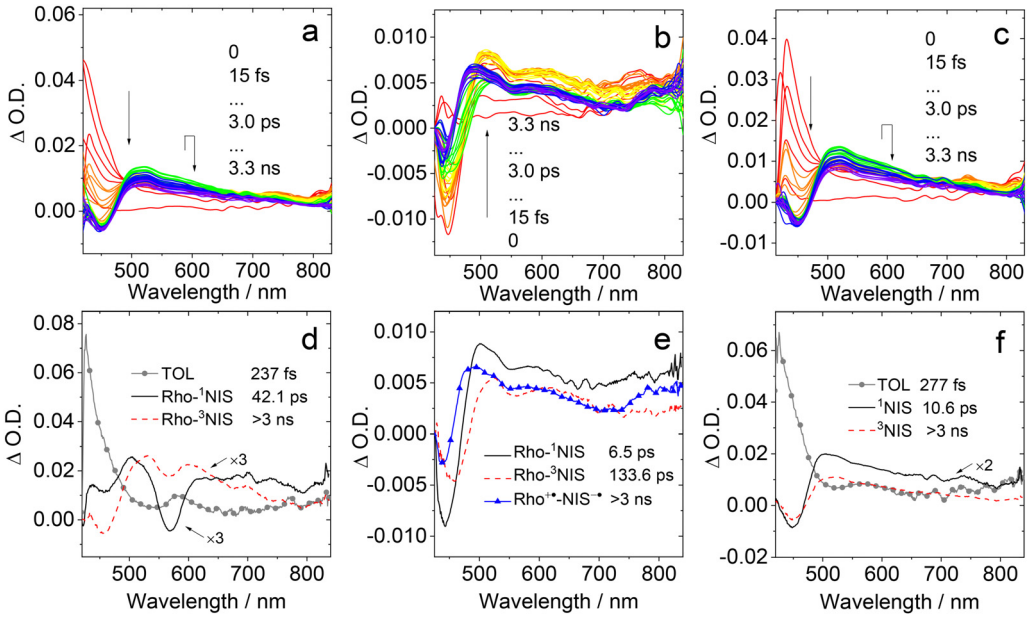

Fig. 5 Femtosecond transient absorption (fs-TA) spectra of **Rho-NIS** in (a) TOL and (b) ACN. The related evolution associated difference spectra (EADS) in (d) TOL and (e) ACN for **Rho-NIS**. (c) fs-TA spectra and (f) the related EADS of **NIS** in TOL. EADS were obtained from target analysis with the sequential model. λ_{ex} = 355 nm. c = 1.0 × 10^{-4} M, 25 °C.

of the solvent, Fig. 5d). The first species can be assigned as a locally excited singlet state of ^{1}**NIS** by comparison with the spectra of **NIS** reported in Fig. 5f. After 42.1 ps, the second species was formed with absorption bands at 530 nm and 602 nm, which is attributed to the ^{3}**NIS** state of **Rho-NIS** and the same in the ns TA spectra (see later section). Thus, the process of **Rho-NIS** upon photo-excitation in TOL can be summarized as ^{1}**NIS** → ^{3}**NIS** by SOC-ISC, taking 42.1 ps, which is slightly slower than the ISC kinetics of **NIS** (10.6 ps). No CS state was observed. In ACN, initial EADS showed the appearance of ESA bands peaked at 500 nm and 760 nm, which can be assigned to the ^{1}**NIS** state by comparison with the spectrum of **NIS** (Fig. 5e). After 6.5 ps, the ESA band at 500 nm was red shifted to 525 nm and the ESA band at 760 nm disappeared. This species is attributed to the ^{3}**NIS** state of **Rho-NIS**, which is similar to the fs-TA signal of **Rho-NIS** and **NIS** observed in TOL on a long-timescale. After 133.6 ps, the transient spectrum evolved significantly, with the appearance of two positive bands peaked at 485 nm and 780 nm, respectively. The comparison with the absorption spectra of **NIS**$^{\bullet-}$ generated by chemical reduction (Fig. 4) allowed us to assign these bands to the **NIS**$^{\bullet-}$ radical anion, and this species is attributed to the CS state (*i.e.*, **Rho**$^{\bullet+}$**-NIS**$^{\bullet-}$). The final spectral component lived well beyond the time explored with the fs-TA measurement (3 ns), in accordance with the ns-TA spectra result. Thus, the photophysical process for **Rho-NIS** in ACN is ^{1}**NIS** → ^{3}**NIS** → CS state. Therefore, electron spin control was realized in formation of the long-lived CS state. This is similar to the previously reported **Rho-NI** without thionated NI.[40] The difference is that ISC is achieved with the thionated NI moiety not by the SOCT-ISC. It should be noted that the CS state energy level is dependent on the solvent polarity, whereas the ^{3}LE state is much less dependent on it.[89]

The fs-TA spectra of **Rho-NIS** in the presence of acid were also studied (Fig. S23 and S24, ESI†). In TOL, based on the EADS analysis, the first species showed the ESA band peaked at 440 nm and GSB band peaked at 560 nm (Fig. S23, ESI†). Moreover, the strong negative bands in the range of 570–590 nm are attributed to both the GSB and stimulated emission (SE) bands due to the fact that the fluorescence of the open form of rhodamine has maximum at 575 nm. An SE band in the range of 600–680 nm was also observed. Therefore, the first species is attributed to the singlet state of the open form of rhodamine, *i.e.*, ^{1}**Rho-o**. After 23.7 ps, ESA bands centred at 530 nm and beyond 590 nm were observed. It should be noted that this positive band may cover the range of 480–700 nm, but this band is distorted by the GSB band. It shares the same characteristics with **Rho-**^{3}**NIS** observed in TOL without the addition of acid. Consequently, this species is assigned as ^{3}**NIS** and it did not decay to the baseline in the time detection window of fs-TA (3 ns), which is same as the that observed in the ns-TA spectra initially. In MeOH, similar results were observed (Fig. S24, ESI†). The lifetime of ^{1}**Rho-o** was 46.5 ps. The mechanism by which the energy transferred from the ^{1}**Rho-o** to ^{3}**NIS** state is unclear. It is known that the ISC process of the **Rho-o** unit is not efficient,[70] and therefore it is unlikely that the mechanism involves the formation of the T_1 state of the **Rho-o** unit.[90] This is probably a singlet–triplet energy transfer (STET) or ^{3}**NIS** state generated by charge recombination (CR) from the CS state (*i.e.*, **Rho-o**$^{\bullet+}$**-NIS**$^{\bullet-}$); however, the CS state could not be observed due to the short lifetime. Based on the electrochemical results, charge transfer

from **Rho-o** to **NIS** with S_1 state of **Rho-o** (E_S = 2.19 eV) as a precursor is a thermodynamics allowed process (ΔG^0_{CS} = −0.15 eV, E_{CS} = 2.04 eV in TOL and ΔG^0_{CS} = −0.53 eV, E_{CS} = 1.66 eV in MeOH). Also, the energy of the ^{3}**NIS** state (E_T = 1.68 eV) is close or lower than that of the CS state.

Nanosecond transient absorption (ns-TA) spectra

To study the long-lived transient species formed in **Rho-NIS** upon photoexcitation, the ns-TA spectra of the compounds were studied (Fig. 6). In the case of **Rho-NIS** upon photoexcitation in TOL, a GSB band centered at 450 nm was observed, as well as a positive absorption band in the range beyond 500 nm (Fig. 6a). It should be noted that this positive band may also cover the range of 350–550 nm, but it is probably distorted by the GSB band. The reference compound **NIS** was also studied, and a similar spectral feature was observed (Fig. 6c); thus, the positive absorption band of **Rho-NIS** is attributed to the ^{3}**NIS** state not a CS state. Interestingly, the lifetime of the ^{3}**NIS** state of **Rho-NIS** was determined to be 0.38 μs (Fig. 6e), which is slightly longer than that of the reference **NIS** of 0.20 μs in TOL (Fig. 6g). The slightly longer ^{3}LE state lifetime of **Rho-NIS** compared to **NIS** is attributed to the acetylation of the amino group in **Rho-NIS**, which is supported by the slightly longer triplet state lifetime of **NIS-NHAc** (0.57 μs) than **NIS** (Fig. S38, ESI†). It should be noted that these ^{3}**NIS** state lifetimes are much shorter than the triplet state lifetime of the native NI moiety (unthionated, 67 μs).[66,91] In ACN, **Rho-NIS** showed ESA bands at 480 nm and 780 nm (Fig. 6b), which are different from that of the spectra observed in TOL, but the results are similar to the absorption spectra of **NIS**$^{\bullet-}$ generated by chemical reduction (Fig. 4), demonstrating the formation of a CS state in this case. The lifetime of the CS state was determined to be 0.21 μs (Fig. 6f). It should be noted that the CS state we observed with ns-TA spectra is most likely a ^{3}CS state because the fluorescence of the **Rho-NIS** state was quenched, and no emission was observed from ^{1}CS, given that its lifetime was too short and could not be determined using the ns-TA spectrometer. It should be noted that the ^{1}CS state and ^{3}CS state may share similar optical absorption character.[92–95] The ^{3}CS state of **Rho-NIS** is generated from ^{3}**NIS** by electron spin control based on the fs-TA spectral studies, *i.e.*, the photophysical process for **Rho-NIS** in ACN is ^{1}**NIS** → ^{3}**NIS** → ^{3}CS state. The quantum yield of the charge separation (Φ_{CS}) was determined using a relative method with anthracene as a standard (for details, refer to the ESI†). In ACN, the Φ_{CS} of **Rho-NIS** was determined to be 97%, which is higher than that of the previously reported **Rho-NI** (49% in HEX).[40] We propose that the thionation of the carbonyl group in **Rho-NIS** induces efficient ISC, and further generates the CS state efficiently *via* the electron spin control effect. Alternatively, the triplet state lifetime of **NIS** in ACN was shortened to 0.06 μs (Fig. S35, ESI†). Interestingly, **NIS-NH$_2$** showed different ESA bands and longer triplet state lifetime (*ca.* 6 μs, Fig. 6d and h) compared with **NIS** and **Rho-NIS**, and it was less dependent on the solvent polarity (Fig. S37, ESI†).

Concerning the reported **Rho-NI** dyad,[40] without thionation of the carbonyl group of the NI unit, the NI moiety showed a higher triplet state energy (E_T = 2.21 eV) and weaker electron-accepting ability (E_{red} = −1.75 V) compared with the **NIS** moiety (E_T = 1.68 eV, E_{red} = −1.09 V). This led to the higher energy of the CS state (2.12 eV) and longer lifetime of the CS state (0.94 μs in HEX) by electron spin control strategy for the previously reported **Rho-NI** dyad.[40] The photophysical processes of **Rho-NI** in HEX upon photoexcitation are summarized as ^{1}NI → ^{1}CS → ^{3}NI → ^{3}CS. The lifetime of the CS state of **Rho-NI** was 0.62 μs in TOL and no CS state was observed in ACN. In contrast, for **Rho-NIS**, the relative energy order of the CS and ^{3}LE states is

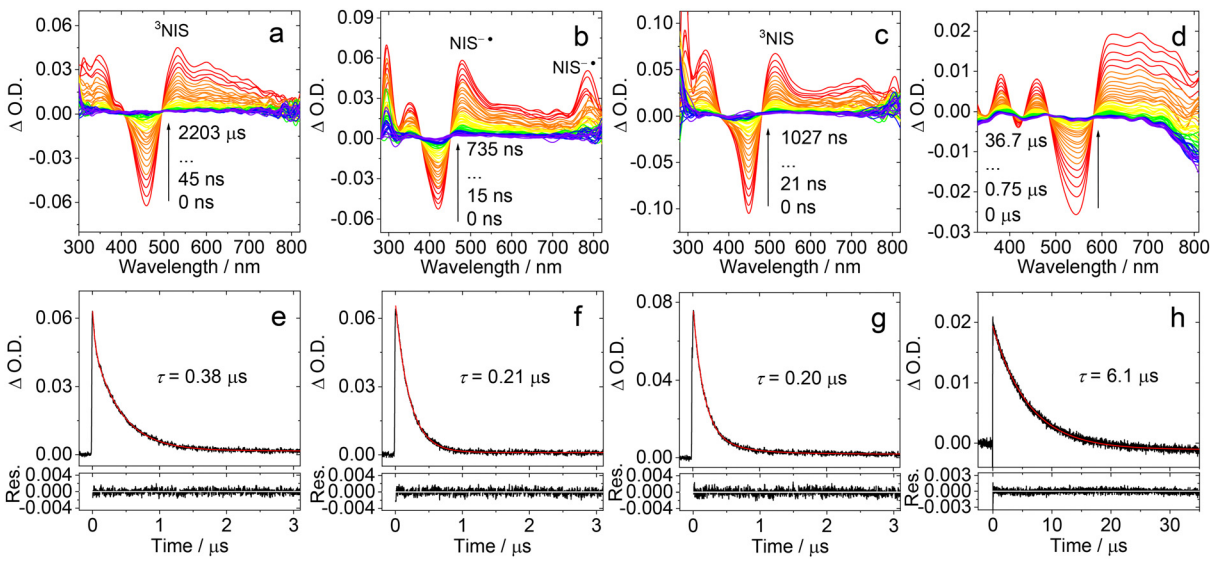

Fig. 6 Nanosecond transient absorption spectra of **Rho-NIS** in deaerated (a) TOL and (b) ACN and (c) **NIS** and (d) **NIS-NH$_2$** in deaerated TOL. Decay traces of **Rho-NIS** in deaerated (e) TOL at 530 nm and (f) ACN at 480 nm and (g) **NIS** at 520 nm and (h) **NIS-NH$_2$** at 630 nm in deaerated TOL. Excited with nanosecond pulsed laser. λ_{ex} = 355 nm for **Rho-NIS** and **NIS**. λ_{ex} = 530 nm for **NIS-NH$_2$**. *c*[**Rho-NIS**] = 4.0 × 10^{-5} M. *c*[**NIS**, **NIS-NH$_2$**] = 2.0 × 10^{-5} M. 25 °C.

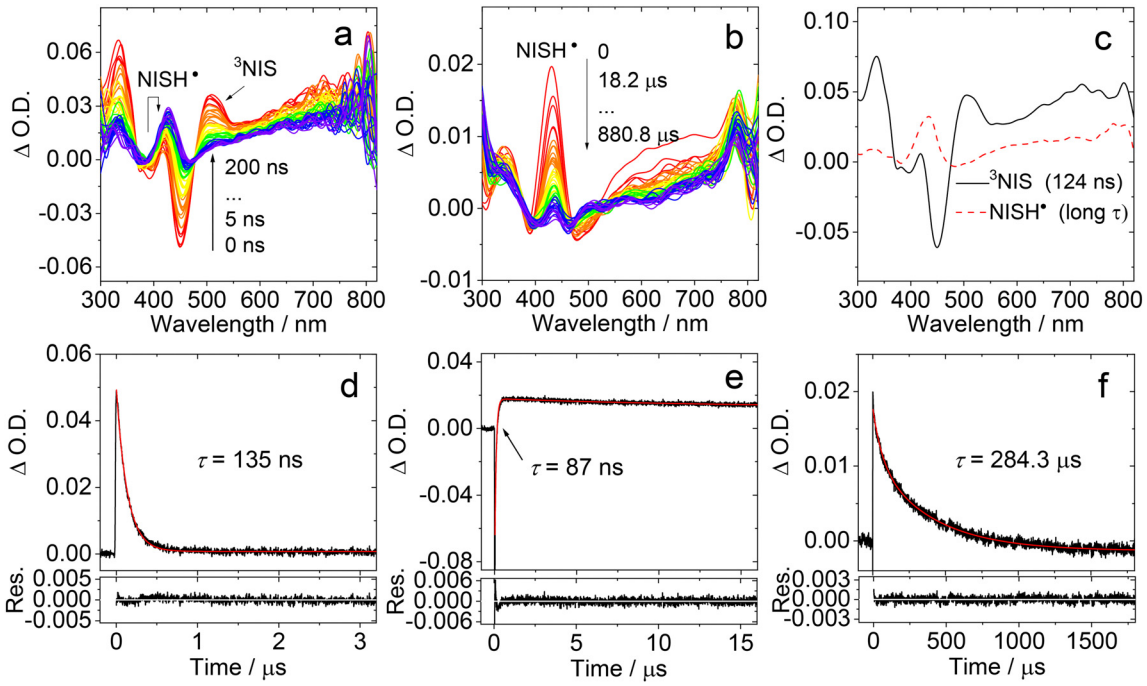

Fig. 7 Nanosecond transient absorption spectra of **NIS** in deaerated isopropanol in (a) short and (b) long delay time range to study the hydrogen abstraction. (c) Related evolution-associated difference spectrum (EADS) obtained from the target analysis with the sequential model for **NIS**. (d) Decay traces of **NIS** at 520 nm and at 430 nm in (e) short and (f) long timescale, excited with nanosecond pulsed laser. λ_{ex} = 355 nm. $c = 3.0 \times 10^{-5}$ M, 25 °C.

dependent on the solvent polarity. In the low-polarity TOL solvent, the ^{3}**NIS** state (τ_T = 0.38 μs) as the lowest triplet state was observed, in the polar solvent ACN and the CS state with the lifetime of 0.21 μs was generated by electron spin control, *i.e.*, the photophysical process of **Rho-NIS** in ACN is ^{1}**NIS** → ^{3}**NIS** → ^{3}CS.

Given that the transient absorption spectra show that the lowest triplet state of **NIS** has ^{3}n-π* character,[51] the ns-TA spectra of **NIS** were also measured in the protic polar solvent isopropanol (IPA) (Fig. 7). In the short delay time range, the ^{3}**NIS** state showing an ESA band centered at 510 nm was observed in deaerated IPA (Fig. 7a). At a longer delay time, an ESA band peaking at 430 nm appeared and increased gradually as the ESA band of the ^{3}**NIS** state decreased (Fig. 7a and b). This is different from the feature of **NIS**$^{\bullet-}$ absorption (485 nm and 780 nm) and can be assigned as NISH$^\bullet$ upon hydrogen abstraction by ^{3}**NIS** from IPA. The evolution of the kinetic trace at 430 nm was monitored, which showed a raised component with the time of 87 ns (Fig. 7e), which is attributed to the accumulation of the NISH$^\bullet$. Also, the lifetime of NISH$^\bullet$ was determined to be 284.3 μs (Fig. 7f), which is much longer than that of the ^{3}NIS state (0.2 μs, Fig. 6). To differentiate the species in the transient absorption spectra, EADS by global fitting to the ns-TA spectra with the sequential model were obtained (Fig. 7c). Two species were identified, where the first species is the ^{3}**NIS** state with the lifetime of 124 ns, which is close to that monitored at 520 nm (135 ns, Fig. 7d). The second species is the long-lived NISH$^\bullet$ (284.3 μs). The result of hydrogen abstraction between the photoexcited state of **NIS** in IPA indicates the n–π* character of the lowest-lying triplet state of **NIS**.[96] Under an air atmosphere (aerated IPA), only the ^{3}**NIS** state was observed and its lifetime was much shorter (0.07 μs, Fig. S43, ESI†). This short excited-state lifetime makes the hydrogen abstraction process unlikely.[97,98] Similar results were observed for **Rho-NIS** and **NIS-NHAc** in deaerated IPA upon photoexcitation (Fig. S42 and S45, respectively, ESI†), indicating the n–π* character of the triplet state. Long-lived NISH$^\bullet$ (25.9 μs for **Rho-NIS** and 349.2 μs for **NIS-NHAc**) was generated together with the decay of ^{3}**NIS**. However, **NIS-NH$_2$** showed the same ns-TA spectra in IPA and other aprotic solvents, proving that it has ^{3}π–π* character or weak ^{3}n-π* character (Fig. S44, ESI†). This is supported by its longer triplet state lifetime (Fig. 6h, 6.1 μs). NI was also observed to undergo hydrogen abstraction by the ^{3}NI state in IPA (Fig. S46, ESI†), resulting in the formation of NIH$^\bullet$ (329.7 μs), which absorbs at 410 nm, in agreement with the reported ns-TA spectra of NIH$^\bullet$ (Fig. S46, ESI†).[98,99] The slow rate of the formation of NIH$^\bullet$ (19.1 μs) is probable due to the weak n–π* character in ^{3}NI, leading to the non-efficient hydrogen abstraction from IPA. Photo-induced hydrogen abstraction, and thus formation of a radical, is potentially useful for the development of new photoinitiators for photopolymerization.[100,101]

In the case of **Rho-NIS**, with the addition of acid, the transformation of the closed form of the rhodamine moiety to the open form occurred, and its ns-TA spectra were studied upon photoexcitation. In TOL, in the presence of TFA, the ^{3}**NIS** state was observed initially (Fig. S33, ESI†). The ESA band in the range of 530–600 nm overlaps with the GSB band originating from the absorption of the rhodamine unit in the open form. As the delay time increased, the ESA band centered at 530 nm

disappeared and the new ESA band in the range of 400–500 nm increased. To identify these different species, global fitting was performed and EADS was obtained (Fig. S33b, ESI†). The first species is assigned as the ^{3}**NIS** state. In the following 460 ns, the second species was formed, which is tentatively attributed to the triplet state of the rhodamine unit in the open form, *i.e.*, ^{3}**Rho-o**, similar to the reported ns-TA spectra of ^{3}**Rho-o**.[74] Therefore, triplet–triplet energy transfer (TTET) occurred from ^{3}**NIS** to ^{3}**Rho-o** within 460 ns. The decay trace monitored at 470 nm has a raised component with a time of 0.60 μs, which is close to the time for TTET determined from EADS (0.46 μs). The decay trace at 560 nm has a biexponential feature and the lifetime is 0.62 μs (32%)/9.4 μs (68%). The component with the lifetime of 0.62 μs is attributed to the decay of ^{3}**NIS**, *i.e.*, TTET process. The component with the lifetime of 9.4 μs is attributed to the decay of ^{3}**Rho-o**. Notably, the ^{3}**Rho-o** state energy is reported to be 1.73 eV (estimated by TDDFT calculations),[77,90] which is slightly higher than the energy of the ^{3}**NIS** state (1.68 eV). This is probably because the TDDFT calculation overestimates the energy of the ^{3}**Rho-o** state. In MeOH, in the presence of TFA, a similar TTET process from ^{3}**NIS** to ^{3}**Rho-o** was observed within 0.11 μs and the lifetime of ^{3}**Rho-o** was 13.6 μs (Fig. S30, ESI†). It should be noted that in the absence of TFA, the CS state of **Rho-NIS** with the lifetime of 0.19 μs was observed in MeOH (Fig. S27, ESI†). These results demonstrate that the **Rho-NIS** dyad with the **Rho** unit in the open form shows different photophysical properties compared to **Rho-NIS** with the **Rho** unit in the close form. This external stimuli-responsive photophysical property may be used to develop functional materials.[102,103]

Time-resolved electron paramagnetic resonance (TREPR) spectroscopy

To study the transient paramagnetic species of the compounds formed upon photoexcitation, a TREPR spectral study was carried out, which is useful to discriminate between the ^{3}CS and ^{3}LE states and the ^{3}CS state and the spin-correlated radical pair.[12,35,104–107] In the case of **NIS** and **Rho-NIS**, no TREPR spectra were observed in frozen solution at 80 K, even at 10 K, with an X- and Q-band spectrometer. This is probably the result of the short triplet state lifetime (0.20 μs for **NIS** and 0.38 μs for **Rho-NIS**) and the fast spin relaxation. The triplet-state TREPR spectra at the Q-band of **NIS-NH$_2$** was observed with the electron spin polarization (ESP) phase pattern of (e, e, e, a, a, a) (Fig. 8a and b). The spectrum at Q-band was well described by the EasySpin package (Fig. 8b). The triplet spectra exhibit a forbidden transition in the X-band (Fig. S49, ESI†).

An isotropic *g*-tensor of 2.0070 was used to simulate the TREPR spectrum of **NIS-NH$_2$** (Fig. 8b). The results of the simulations are presented in Table 3. The zero-field splitting (ZFS) parameters $|D|$ of 6165 MHz and E of −1233 MHz were obtained by simulation of the TREPR spectra of **NIS-NH$_2$**, which are both larger than that of NI with $|D|$ of 2475 MHz and $|E|$ of 135 MHz, and its analogue without thionation as that in **NIS-NH$_2$**, *i.e.*, NI-NH-Br, gave $|D|$ of 2314 MHz and $|E|$ of 193 MHz.[66,88] The large ZFS parameter $|D|$ of **NIS-NH$_2$** indicates

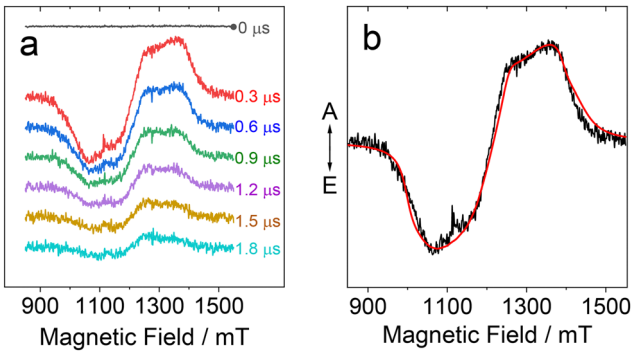

Fig. 8 TREPR spectra of **NIS-NH$_2$** measured with Q-band EPR spectrometer excited with 532 nm laser with energy 10 mJ per pulse (a) at different delay time and (b) at 0.3 μs in TOL/2-MeTHF (1 : 3, v/v) at 80 K. The simulation (red curve in b) was performed with EasySpin package. c = 1.0×10^{-4} M.

Table 3 Zero-field splitting parameters ($|D|$ and E) and relative populations $P_{x,y,z}$ of the spin states at zero magnetic field of the compounds[a]

	$\|D\|$ (MHz)	$\|E\|$ (MHz)	P_x	P_y	P_z	*g*-Factor
NIS-NH$_2$	6165	1233	0.50	0.50	0	2.0070
NI[b]	2745	135	0.16	0.84	0	—[c]
NI-NH-Br[d]	2314	193	0	0.38	0.62	2.0050

[a] Obtained from simulations of the triplet-state TREPR spectra of the indicated molecules at 80 K. P_i is the relative population of the *i*-th ZFS state. [b] Literature values, see ref. 66. [c] Not reported. [d] Literature values, see ref. 88.

that its triplet state has mixed n–π* and π–π* character.[108] This led to the shorter triplet state lifetime of **NIS-NH$_2$** (6.1 μs) compared to compound **4** (17.5 μs, obtained by TTET, Fig. S47, ESI†). The relative population rates of the three sublevels of the triplet state of **NIS-NH$_2$** at zero magnetic field are $P_x : P_y : P_z$ = 0.5 : 0.5 : 0.

It is known that 9,10-anthraquinone (AQ) has a T_1 state with n–π* character, ZFS D of −9000 MHz, and E of 160 MHz.[108] In the case of 9,10-diazaphenanthrene (DAP), the T_1 state was assigned as the n–π* state in the single crystal of biphenyl, and the ZFS D and E parameters were determined to be −4011 MHz and 2667 MHz, respectively.[109] In polar solvents, such as 2,2,2-trifluoroethanol, the T_1 state of DAP has π–π* character, and the D and E values are −2788 MHz and 1199 MHz, respectively. Furthermore, the T_1 state of pyridazine has n–π* character and its ZFS D and E parameters were determined to be −4137 MHz and 3478 MHz, respectively.[110,111] These results demonstrate that the compounds with a T_1 state having n–π* character may give a large ZFS parameter D than the corresponding ^{3}n–π* state.

Theoretical computations

To rationalize the photophysical property of the compounds, theoretical computations were performed. The ground state geometry of the compounds was optimized by DFT calculations (Fig. S50, ESI†). In the case of **Rho-NIS**, the dihedral angle

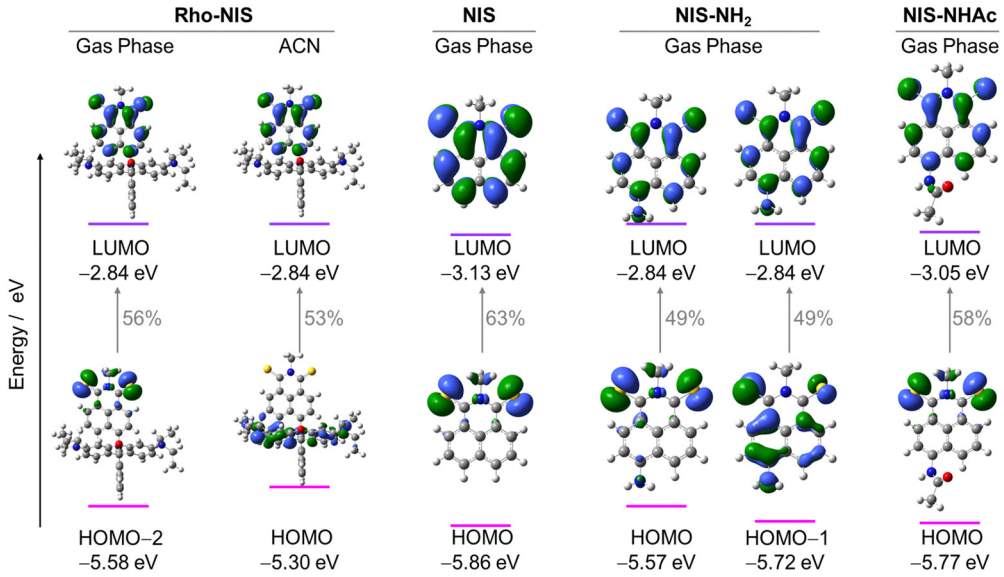

Fig. 9 Selected frontier molecular orbitals contributing to the T_1 states of the compounds (isovalue = 0.04). The orbital transition probability and energy of T_1 states are also shown. Calculation was performed by DFT at the B3LYP/6-31G(d) level with Gaussian 09.

between the π-conjugation planes of the rhodamine xanthene moiety and **NIS** is 61.6°, which is slightly different from the molecular structure determined by the single-crystal X-ray diffraction experiments (53.0°), and the difference probably results from the packing effect in the single crystal. The centroid-to-centroid distance between xanthene and the **NIS** moieties is 5.6 Å, which is close to the previously reported dyads without thionation of the NI unit.[40] The frontier molecular orbitals (MOs) of the dyads were studied (Fig. 9). The highest occupied molecular orbital (HOMO) of **Rho-NIS** is confined on the **Rho** moiety and the lowest unoccupied molecular orbital (LUMO) is confined on the **NIS** moiety. There is negligible delocalization on these two moieties for both MOs, which is in agreement with the molecular structure design rationale to obtain the CS state upon photoexcitation.

The frontier molecular orbitals involved in the T_1 states of the compounds were examined (Fig. 9). In the gas phase, the orbitals involved in the transition of the T_1 state **Rho-NIS** and **NIS** and **NIS-NHAc** mainly have n–π* character. This is supported by the short triplet excited state of these compounds, as well as the hydrogen abstraction properties observed in their ns-TA spectra. The MOs of the T_1 state of **NIS** have n–π* character and are similar to the T_1 state of 9,10-diazaphenanthrene (DAP), which has a pure n–π* T_1 state.[109] However, for **NIS-NH$_2$**, the orbital transition of the T_1 state is a mixture of n–π* and π–π* in nearly equal proportion (49%). This is in agreement with the longer triplet excited state lifetime of 6.1 μs (Fig. 6h).

The T_1 states of the compounds were also analysed by the natural transition orbital (NTO, Fig. S54, ESI†). For all these compounds, the contribution from the NTO pair with the largest eigenvalue is over 95%. In the gas phase, the hole involved in the T_1 state of **NIS** spreads mainly over the two sulphur atoms and the contribution of the sulphur atoms to the hole is over 70%, whereas the particle is spread over the whole molecule (Fig. S54 and S55, ESI†), which indicates that the T_1 state of **NIS** mainly has n–π* character. Similar results were observed for **Rho-NIS** and **NIS-NHAc**, which have similar T_1 states with n–π* character. However, in the case of **NIS-NH$_2$**, the hole involved in the T_1 state spread over the two sulphur atoms as well as the aromatic framework, and the contribution of the two sulphur atoms to the hole is 27.0% and 15.3%, respectively, and the sum of their contribution is less than 50% (Fig. S54 and S55, ESI†). The particle is spread over the whole molecular structure. Therefore, in the case of **NIS-NH$_2$**, the T_1 state is an admixture of n–π* and π–π* character based on the NTO analysis, which is in accordance with the analysis based on frontier molecular orbitals involved in the T_1 states and the ns-TA spectral results.

The electron spin density surface of the T_1 state of **Rho-NIS** in the gas phase, TOL and ACN was studied (Fig. 10) to corroborate the ns-TA spectral observation. In the gas phase and TOL, the electron spin density was confined on the thionated NI unit, and the sulfur atoms contributed

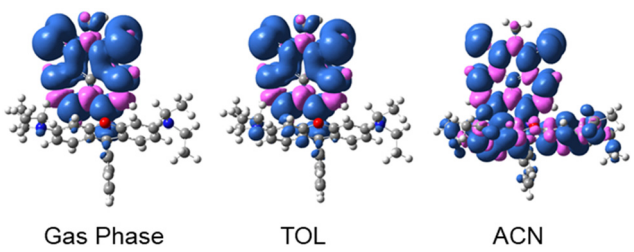

Fig. 10 Isosurfaces of spin density at the optimized triplet state geometries of **Rho-NIS** in the gas phase, TOL and ACN (isovalue = 0.0004), respectively. Calculation was performed by DFT method at the UB3LYP/6-31G(d) level with Gaussian 09.

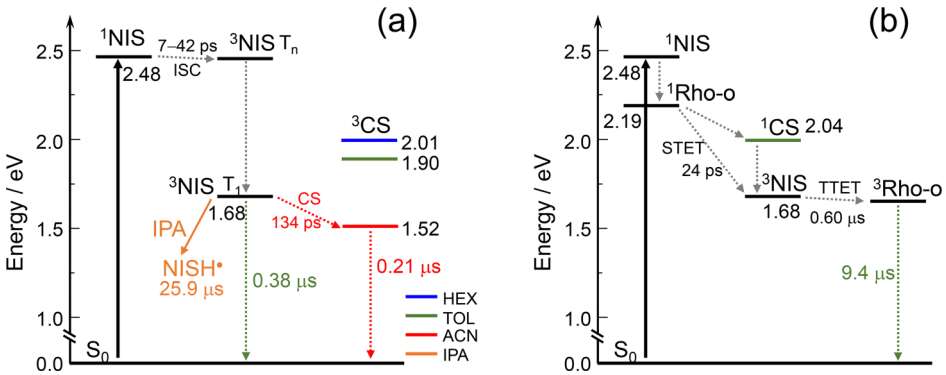

Scheme 2 Simplified Jablonski diagram illustrating the photophysical processes involved in **Rho-NIS** in the (a) absence and (b) presence of acid. The energy of the excited singlet states is estimated by UV-vis absorption spectra and fluorescence spectra. The energy of the triplet state is estimated by the 00 transition based on the phosphorescence emission spectra and the energy of CT states is obtained by electrochemical calculation. The number of the superscript denotes the spin multiplicity. IPA stands for isopropanol.

significantly, and thus we conclude that it is a triplet state with significant n–π* character, not a pure ^{3}CS state (with the closed ring structure of rhodamine as the electron donor). This is in agreement with the ns-TA spectral results. However, in ACN, the electron spin density of the T_1 state was delocalized on both the thionated NI and rhodamine units. Notably, there was no ^{3}**NIS** and ^{3}**Rho** excited-state equilibrium due to the large energy gap between the triplet state of **NIS** (1.68 eV) and rhodamine moieties (3.36 eV).[77] This result suggests that a ^{3}CS state may be formed in ACN upon photoexcitation, which is in agreement with the ns-TA spectral studies (Fig. 6).

Based on the above-mentioned results, the energy diagram of **Rho-NIS** was constructed (Scheme 2). In the absence of acid, upon the photoexcitation of the **NIS** moiety in both TOL and ACN, the singlet excited state of **Rho-NIS** (*i.e.*, ^{1}**NIS** state) is populated. Then, in TOL, fast ISC (42 ps) produces the triplet state localized on the **NIS** moiety (^{3}**NIS**) with the lifetime of 0.38 μs. The ^{3}**NIS** state has the n–π* character, leading to hydrogen abstraction from the protic solvent to generate the long-lived NISH• (25.9 μs). In ACN, ^{3}**NIS** was produced by fast ISC (7 ps) from the ^{1}**NIS** state, and then the charge separation (CS) from the ^{3}**NIS** state takes 134 ps to generate the ^{3}CS state. The ^{3}CS state lifetime is 0.21 μs. The photophysical process of **Rho-NIS** in ACN upon photoexcitation is ^{1}**NIS** → ^{3}**NIS** → ^{3}CS. In the presence of acid (Scheme 2b), upon photoexcitation, the singlet of rhodamine in the open form (*i.e.*, ^{1}**Rho-o** state) was populated, and then the ^{3}**NIS** state was formed within 24 ps by singlet–triplet energy transfer or rapid charge recombination from the CS state (*i.e.*, **Rho-o**$^{\bullet+}$-**NIS**$^{\bullet-}$, generated by charge transfer from ^{1}**Rho-o** state). Subsequently, TTET from the ^{3}**NIS** state takes 0.6 μs, leading to the formation of the ^{3}**Rho-o** state with the lifetime of 9.4 μs.

Conclusions

In conclusion, using the rhodamine (**Rho**) moiety as an electron donor, having the ability to undergo a reversible transformation of spirolactam ↔ open form amide structure, and thionated naphthalimide (**NIS**) as an electron acceptor, we prepared a compact, orthogonal electron donor–acceptor dyad **Rho-NIS**. Our aim was to access the long-lived triplet charge separation (^{3}CS) state based on the electron spin control approach, and the purpose of thionation was to enhance the ISC to produce the ^{3}**NIS** state. **Rho** (lactam form) was attached to **NIS** at the 4-position *via* a single C–N bond. The transient absorption (TA) spectra showed that intersystem crossing (ISC) of ^{1}**NIS** → ^{3}**NIS** occurs rapidly in different solvents (7–42 ps) upon photoexcitation, which was assigned to the spin orbit coupling ISC (SOC-ISC) mechanism due to the ^{3}n-π* character of the T_1 state of the **NIS** moiety. In TOL, a triplet state localized on the **NIS** moiety (^{3}**NIS**) was observed for **Rho-NIS** with the lifetime of 0.38 μs. Also, the ^{3}**NIS** state has the ability to undergo hydrogen abstraction in protic solvents due to its n–π* character and generates the long-lived NISH• (25.9 μs). Alternatively, the long-lived CS state was observed in ACN, with the lifetime of 0.21 μs and the quantum yield of the CS state (Φ_{CS}) was high (97%). The relative energy of the ^{3}CS and ^{3}LE states changed in solvents with different polarity. The long-lived CS state of the dyad was based on the electron spin control effect, that is, the generation of the final ^{3}CS state with a triplet precursor (^{3}**NIS** state). For the previously reported analogue **Rho**-naphthalimide (NI) dyad, without thionation of the carbonyl group of the NI unit, the relative energy of the CS and ^{3}LE states was not inverted by a variation in the solvent polarity. The long-lived CS state generated by the electron spin control strategy was observed in both *n*-hexane (HEX, 0.94 μs; Φ_{CS}, 49%) and TOL (0.62 μs), which are longer than the CS state lifetime of **Rho-NIS** in ACN (0.21 μs). However, no CS state was observed for **Rho-NI** in ACN. The current thionation strategy makes the formation of the long-lived ^{3}CS state in ACN and improvement of the Φ_{CS} possible. Furthermore, the effect of the open/closed form of **Rho** on the photophysical process was also studied. In the presence of acid, the **Rho** unit in **Rho-NIS** transformed to the open form (**Rho-o**), which showed a broadband absorption in the visible spectral region (500–650 nm). The ^{3}**NIS** state was formed from the ^{1}**Rho-o** state within 24–47 ps. Then, ^{3}**Rho-o** state (9.4–13.9 μs) was formed by

triplet–triplet energy transfer (TTET) from the ^{3}**NIS** state within 0.11–0.60 μs. In the time-resolved electron paramagnetic resonance (TREPR) spectra, the triplet state signal of **NIS-NH$_2$** was observed and the zero-field splitting (ZFS) parameters $|D|$ and E of **NIS-NH$_2$** were determined to be 6165 MHz and −1233 MHz, respectively. Compared to the NI compound with a long triplet state lifetime (67.2 μs), $|D|$ of 2475 MHz and $|E|$ of 135 MHz, the large $|D|$ value of **NIS-NH$_2$** demonstrates that its triplet state has the mixed character of n–π* and π–π*, leading to its short triplet state lifetime (6.1 μs). Thus, these results indicate that thionation may significantly shorten the triplet state lifetime and this strategy should be carefully used to design heavy atom-free triplet photosensitizers to realize the desirable long triplet state lifetime. These results are also useful for understanding the charge transfer and access to the long-lived CS state in compact electron donor/acceptor dyads.

Author contributions

X. X., T. M. and A. A. S. contributed equally to this work.

Conflicts of interest

There are no conflicts to declare.

Acknowledgements

J. Z. thanks the NSFC (U2001222), the Research and Innovation Team Project of Dalian University of Technology (DUT2022TB10), the Fundamental Research Funds for the Central Universities (DUT22LAB610), and the State Key Laboratory of Fine Chemicals for financial support. A. A. S. and V. K. V. acknowledge financial support from the government assignment for FRC Kazan Scientific Center of RAS.

Notes and references

1 D. M. Guldi, *Chem. Commun.*, 2000, 321–327.
2 J. W. Verhoeven, H. J. van Ramesdonk, M. M. Groeneveld, A. C. Benniston and A. Harriman, *ChemPhysChem*, 2005, **6**, 2251–2260.
3 J. W. Verhoeven, *J. Photochem. Photobiol., C*, 2006, **7**, 40–60.
4 S. Fukuzumi, *Pure Appl. Chem.*, 2007, **79**, 981–991.
5 D. Veldman, S. M. A. Chopin, S. C. J. Meskers and R. A. J. Janssen, *J. Phys. Chem. A*, 2008, **112**, 8617–8632.
6 O. Kei and F. Shunichi, *Bull. Chem. Soc. Jpn.*, 2009, **82**, 303–315.
7 S. Suzuki, M. Kozaki, K. Nozaki and K. Okada, *J. Photochem. Photobiol., C*, 2011, **12**, 269–292.
8 E. Vauthey, *ChemPhysChem*, 2012, **13**, 2001–2011.
9 M. Delor, T. Keane, P. A. Scattergood, I. V. Sazanovich, G. M. Greetham, M. Towrie, A. J. H. M. Meijer and J. A. Weinstein, *Nat. Chem.*, 2015, **7**, 689–695.
10 G. N. Lim, C. O. Obondi and F. D'Souza, *Angew. Chem., Int. Ed.*, 2016, **55**, 11517–11521.
11 Y. Hou, X. Zhang, K. Chen, D. Liu, Z. Wang, Q. Liu, J. Zhao and A. Barbon, *J. Mater. Chem. C*, 2019, **7**, 12048–12074.
12 N. Zarrabi, B. J. Bayard, S. Seetharaman, N. Holzer, P. Karr, S. Ciuti, A. Barbon, M. Di Valentin, A. van der Est, F. D'Souza and P. K. Poddutoori, *Phys. Chem. Chem. Phys.*, 2021, **23**, 960–970.
13 M. Lv, X. Lu, Y. Jiang, M. E. Sandoval-Salinas, D. Casanova, H. Sun, Z. Sun, J. Xu, Y. Yang and J. Chen, *Angew. Chem., Int. Ed.*, 2022, **61**, e202113190.
14 X. Niu, K. Tajima, J. Kong, M. Tao, N. Fukui, Z. Kuang, H. Shinokubo and A. Xia, *Phys. Chem. Chem. Phys.*, 2022, **24**, 14007–14015.
15 H. Imahori, *Bull. Chem. Soc. Jpn.*, 2023, **96**, 339–352.
16 S. M. Sartor, Y. M. Lattke, B. G. McCarthy, G. M. Miyake and N. H. Damrauer, *J. Phys. Chem. A*, 2019, **123**, 4727–4736.
17 S. Suzuki, Y. Matsumoto, M. Tsubamoto, R. Sugimura, M. Kozaki, K. Kimoto, M. Iwamura, K. Nozaki, N. Senju, C. Uragami, H. Hashimoto, Y. Muramatsu, A. Konno and K. Okada, *Phys. Chem. Chem. Phys.*, 2013, **15**, 8088–8094.
18 A. N. Bartynski, M. Gruber, S. Das, S. Rangan, S. Mollinger, C. Trinh, S. E. Bradforth, K. Vandewal, A. Salleo, R. A. Bartynski, W. Bruetting and M. E. Thompson, *J. Am. Chem. Soc.*, 2015, **137**, 5397–5405.
19 E. Salvadori, N. Luke, J. Shaikh, A. Leventis, H. Bronstein, C. W. M. Kay and T. M. Clarke, *J. Mater. Chem. A*, 2017, **5**, 24335–24343.
20 D. Lee, J. Lee, D. H. Sin, S. G. Han, H. Lee, W. Choi, H. Kim, J. Noh, J. Mun, W. Sung, S. W. Kim, B. G. Jeong, S. H. Kim, J. Rho, M. S. Jeong and K. Cho, *J. Phys. Chem. C*, 2022, **126**, 3171–3179.
21 S. Callaghan, M. A. Filatov, H. Savoie, R. W. Boyle and M. O. Senge, *Photochem. Photobiol. Sci.*, 2019, **18**, 495–504.
22 Y. Im, S. Y. Byun, J. H. Kim, D. R. Lee, C. S. Oh, K. S. Yook and J. Y. Lee, *Adv. Funct. Mater.*, 2017, **27**, 1603007.
23 Z. Yang, Z. Mao, Z. Xie, Y. Zhang, S. Liu, J. Zhao, J. Xu, Z. Chi and M. P. Aldred, *Chem. Soc. Rev.*, 2017, **46**, 915–1016.
24 F. Ni, N. Li, L. Zhan and C. Yang, *Adv. Opt. Mater.*, 2020, **8**, 1902187.
25 Y. Xu, P. Xu, D. Hu and Y. Ma, *Chem. Soc. Rev.*, 2021, **50**, 1030–1069.
26 L. Chen, W.-C. Chen, Z. Yang, J.-H. Tan, S. Ji, H.-L. Zhang, Y. Huo and C.-S. Lee, *J. Mater. Chem. C*, 2021, **9**, 17233–17264.
27 H. Kotani, K. Ohkubo and S. Fukuzumi, *Faraday Discuss.*, 2012, **155**, 89–102.
28 V. M. Blas-Ferrando, J. Ortiz, K. Ohkubo, S. Fukuzumi, F. Fernández-Lázaro and Á. Sastre-Santos, *Chem. Sci.*, 2014, **5**, 4785–4793.
29 R. A. Marcus, *Angew. Chem., Int. Ed. Engl.*, 1993, **32**, 1111–1121.
30 D. I. Schuster, P. Cheng, P. D. Jarowski, D. M. Guldi, C. Luo, L. Echegoyen, S. Pyo, A. R. Holzwarth, S. E. Braslavsky, R. M. Williams and G. Klihm, *J. Am. Chem. Soc.*, 2004, **126**, 7257–7270.
31 M. Kuss-Petermann and O. S. Wenger, *Angew. Chem., Int. Ed.*, 2016, **55**, 815–819.

32 B. Geiß and C. Lambert, *Chem. Commun.*, 2009, 1670–1672.
33 J. Hankache and O. S. Wenger, *Chem. Commun.*, 2011, **47**, 10145–10147.
34 S. Fukuzumi, H. Kotani, K. Ohkubo, S. Ogo, N. V. Tkachenko and H. Lemmetyinen, *J. Am. Chem. Soc.*, 2004, **126**, 1600–1601.
35 S. Suzuki, R. Sugimura, M. Kozaki, K. Keyaki, K. Nozaki, N. Ikeda, K. Akiyama and K. Okada, *J. Am. Chem. Soc.*, 2009, **131**, 10374–10375.
36 M. Murakami, K. Ohkubo, T. Nanjo, K. Souma, N. Suzuki and S. Fukuzumi, *ChemPhysChem*, 2010, **11**, 2594–2605.
37 Z. E. X. Dance, Q. Mi, D. W. McCamant, M. J. Ahrens, M. A. Ratner and M. R. Wasielewski, *J. Phys. Chem. B*, 2006, **110**, 25163–25173.
38 Y. Kobori, M. Fuki and H. Murai, *J. Phys. Chem. B*, 2010, **114**, 14621–14630.
39 R. Carmieli, A. L. Smeigh, S. M. Mickley Conron, A. K. Thazhathveetil, M. Fuki, Y. Kobori, F. D. Lewis and M. R. Wasielewski, *J. Am. Chem. Soc.*, 2012, **134**, 11251–11260.
40 D. Liu, A. M. El-Zohry, M. Taddei, C. Matt, L. Bussotti, Z. Wang, J. Zhao, O. F. Mohammed, M. Di Donato and S. Weber, *Angew. Chem., Int. Ed.*, 2020, **59**, 11591–11599.
41 S.-H. Lee, C. T.-L. Chan, K. M.-C. Wong, W. H. Lam, W.-M. Kwok and V. W.-W. Yam, *J. Am. Chem. Soc.*, 2014, **136**, 10041–10052.
42 J. E. McGarrah, Y.-J. Kim, M. Hissler and R. Eisenberg, *Inorg. Chem.*, 2001, **40**, 4510–4511.
43 G. Ajayakumar and K. R. Gopidas, *Photochem. Photobiol. Sci.*, 2008, **7**, 826–833.
44 D. R. Subedi, H. B. Gobeze, Y. E. Kandrashkin, P. K. Poddutoori, A. van der Est and F. D'Souza, *Chem. Commun.*, 2020, **56**, 6058–6061.
45 S. I. van Dijk, C. P. Groen, F. Hartl, A. M. Brouwer and J. W. Verhoeven, *J. Am. Chem. Soc.*, 1996, **118**, 8425–8432.
46 C. Trinh, K. Kirlikovali, S. Das, M. E. Ener, H. B. Gray, P. Djurovich, S. E. Bradforth and M. E. Thompson, *J. Phys. Chem. C*, 2014, **118**, 21834–21845.
47 M. A. Filatov, *Org. Biomol. Chem.*, 2020, **18**, 10–27.
48 D. J. Gibbons, A. Farawar, P. Mazzella, S. Leroy-Lhez and R. M. Williams, *Photochem. Photobiol. Sci.*, 2020, **19**, 136–158.
49 A. J. Tilley, R. D. Pensack, T. S. Lee, B. Djukic, G. D. Scholes and D. S. Seferos, *J. Phys. Chem. C*, 2014, **118**, 9996–10004.
50 M. Hussain, J. Zhao, W. Yang, F. Zhong, A. Karatay, H. G. Yaglioglu, E. A. Yildiz and M. Hayvali, *J. Lumin.*, 2017, **192**, 211–217.
51 V.-N. Nguyen, S. Qi, S. Kim, N. Kwon, G. Kim, Y. Yim, S. Park and J. Yoon, *J. Am. Chem. Soc.*, 2019, **141**, 16243–16248.
52 J. R. Palmer, K. A. Wells, J. E. Yarnell, J. M. Favale and F. N. Castellano, *J. Phys. Chem. Lett.*, 2020, **11**, 5092–5099.
53 J. Tang, L. Wang, A. Loredo, C. Cole and H. Xiao, *Chem. Sci.*, 2020, **11**, 6701–6708.
54 T. C. Pham, S. Heo, V.-N. Nguyen, M. W. Lee, J. Yoon and S. Lee, *ACS Appl. Mater. Interfaces*, 2021, **13**, 13949–13957.
55 A. I. Wright, B. M. Kariuki and Y.-L. Wu, *Eur. J. Org. Chem.*, 2021, 4647–4652.
56 N. Pearce, E. S. Davies, R. Horvath, C. R. Pfeiffer, X.-Z. Sun, W. Lewis, J. McMaster, M. W. George and N. R. Champness, *Phys. Chem. Chem. Phys.*, 2018, **20**, 752–764.
57 O. V. Dolomanov, L. J. Bourhis, R. J. Gildea, J. A. K. Howard and H. Puschmann, *J. Appl. Crystallogr.*, 2009, **42**, 339–341.
58 I. H. M. van Stokkum, D. S. Larsen and R. van Grondelle, *Biochim. Biophys. Acta, Bioenerg.*, 2004, **1657**, 82–104.
59 J. J. Snellenburg, S. Laptenok, R. Seger, K. M. Mullen and I. H. M. van Stokkum, *J. Stat. Software*, 2012, **49**, 1–22.
60 S. Stoll and A. Schweiger, *J. Magn. Reson.*, 2006, **178**, 42–55.
61 T. Lu and F. Chen, *J. Comput. Chem.*, 2012, **33**, 580–592.
62 G. W. T. M. J. Frisch, H. B. Schlegel, G. E. Scuseria, M. A. Robb, J. R. Cheeseman, G. Scalmani, V. Barone, B. Mennucci and G. A. Petersson, *et al.*, *Gaussian 09 (Revision A.01)*, Gaussian, Inc., Wallingford CT, 2009.
63 Y.-L. Lee, Y.-T. Chou, B.-K. Su, C.-C. Wu, C.-H. Wang, K.-H. Chang, J.-A. A. Ho and P.-T. Chou, *J. Am. Chem. Soc.*, 2022, **144**, 17249–17260.
64 Q. Qi, L. Huang, R. Yang, J. Li, Q. Qiao, B. Xu, W. Tian, X. Liu and Z. Xu, *Chem. Commun.*, 2019, **55**, 1446–1449.
65 H. Guo, M. L. Muro-Small, S. Ji, J. Zhao and F. N. Castellano, *Inorg. Chem.*, 2010, **49**, 6802–6804.
66 X. Zhang, X. Liu, M. Taddei, L. Bussotti, I. Kurganskii, M. Li, X. Jiang, L. Xing, S. Ji, Y. Huo, J. Zhao, M. Di Donato, Y. Wan, Z. Zhao and M. V. Fedin, *Chem. – Eur. J.*, 2022, **28**, e202200510.
67 L. Cao, X. Liu, X. Zhang, J. Zhao, F. Yu and Y. Wan, *Beilstein J. Org. Chem.*, 2023, **19**, 1028–1046.
68 S. Sasaki, K. Hattori, K. Igawa and G.-I. Konishi, *J. Phys. Chem. A*, 2015, **119**, 4898–4906.
69 M. Hu, A. A. Sukhanov, X. Zhang, A. Elmali, J. Zhao, S. Ji, A. Karatay and V. K. Voronkova, *J. Phys. Chem. B*, 2021, **125**, 4187–4203.
70 M. H. Lee, J. H. Han, J. H. Lee, N. Park, R. Kumar, C. Kang and J. S. Kim, *Angew. Chem., Int. Ed.*, 2013, **52**, 6206–6209.
71 C. Wang and K. M.-C. Wong, *Inorg. Chem.*, 2013, **52**, 13432–13441.
72 P. Majumdar, X. Yuan, S. Li, B. Le Guennic, J. Ma, C. Zhang, D. Jacquemin and J. Zhao, *J. Mater. Chem. B*, 2014, **2**, 2838–2854.
73 Y. Zhao, Y. Ren, H. Li, T. Han, H. Chen and W. Guo, *Dyes Pigm.*, 2016, **132**, 255–261.
74 X. Cui, J. Zhao, A. Karatay, H. G. Yaglioglu, M. Hayvali and B. Küçüköz, *Eur. J. Inorg. Chem.*, 2016, 5079–5088.
75 Q. Qiao, W. Liu, J. Chen, X. Wu, F. Deng, X. Fang, N. Xu, W. Zhou, S. Wu, W. Yin, X. Liu and Z. Xu, *Angew. Chem., Int. Ed.*, 2022, **61**, e202202961.
76 X. Cui, J. Zhao, Z. Lou, S. Li, H. Wu and K.-L. Han, *J. Org. Chem.*, 2015, **80**, 568–581.
77 L. D. Patsenker and Y. Y. Artyukhova, *J. Mol. Struct.*, 2003, **655**, 311–320.
78 R. Ziessel, B. D. Allen, D. B. Rewinska and A. Harriman, *Chem. – Eur. J.*, 2009, **15**, 7382–7393.
79 J. Hankache and O. S. Wenger, *Chem. – Eur. J.*, 2012, **18**, 6443–6447.

80 M. A. Collini, M. B. Thomas, V. Bandi, P. A. Karr and F. D'Souza, *Chem. – Eur. J.*, 2017, **23**, 4450–4461.
81 B. Ventura, A. Bertocco, D. Braga, L. Catalano, S. d'Agostino, F. Grepioni and P. Taddei, *J. Phys. Chem. C*, 2014, **118**, 18646–18658.
82 D. Gosztola, M. P. Niemczyk, W. Svec, A. S. Lukas and M. R. Wasielewski, *J. Phys. Chem. A*, 2000, **104**, 6545–6551.
83 G. Tang, A. A. Sukhanov, J. Zhao, W. Yang, Z. Wang, Q. Liu, V. K. Voronkova, M. Di Donato, D. Escudero and D. Jacquemin, *J. Phys. Chem. C*, 2019, **123**, 30171–30186.
84 X. Xiao, Y. Yan, A. A. Sukhanov, S. Doria, A. Iagatti, L. Bussotti, J. Zhao, M. Di Donato and V. K. Voronkova, *J. Phys. Chem. B*, 2023, **127**, 6982–6998.
85 P. K. Samanta and N. J. English, *J. Phys. Chem. C*, 2020, **124**, 8178–8185.
86 T. Gerbich, H.-C. Schmitt, I. Fischer, R. Mitrić and J. Petersen, *J. Phys. Chem. A*, 2016, **120**, 2089–2095.
87 X. Chen, J. Pang, M. Imran, X. Li, J. Zhao and M. Li, *Photochem. Photobiol. Sci.*, 2021, **20**, 69–85.
88 W. Tian, A. A. Sukhanov, L. Bussotti, J. Pang, J. Zhao, V. K. Voronkova, M. Di Donato and M.-D. Li, *J. Phys. Chem. B*, 2022, **126**, 4364–4378.
89 H. Imahori, M. E. El-Khouly, M. Fujitsuka, O. Ito, Y. Sakata and S. Fukuzumi, *J. Phys. Chem. A*, 2001, **105**, 325–332.
90 K. Xu, Y. Xie, X. Cui, J. Zhao and K. D. Glusac, *J. Phys. Chem. B*, 2015, **119**, 4175–4187.
91 M. Imran, A. A. Sukhanov, P. Maity, A. Elmali, J. Zhao, A. Karatay, O. F. Mohammed and V. K. Voronkova, *J. Phys. Chem. B*, 2021, **125**, 9244–9259.
92 B. K. Rugg, B. T. Phelan, N. E. Horwitz, R. M. Young, M. D. Krzyaniak, M. A. Ratner and M. R. Wasielewski, *J. Am. Chem. Soc.*, 2017, **139**, 15660–15663.
93 D. Mims, J. Herpich, N. N. Lukzen, U. E. Steiner and C. Lambert, *Science*, 2021, **374**, 1470–1474.
94 X. Zhao and J. Zhao, *Chem. Commun.*, 2022, **58**, 7666–7669.
95 X. Zhang, X. Zhao, K. Ye and J. Zhao, *Chem. – Eur. J.*, 2023, **29**, e202203737.
96 M. Shah, N. S. Allen, M. Edge, S. Navaratnam and F. Catalina, *J. Appl. Polym. Sci.*, 1996, **62**, 319–340.
97 A. Samanta, B. Ramachandram and G. Saroja, *J. Photochem. Photobiol., A*, 1996, **101**, 29–32.
98 D. W. Cho, M. Fujitsuka, A. Sugimoto, U. C. Yoon, D. W. Cho and T. Majima, *Phys. Chem. Chem. Phys.*, 2014, **16**, 5779–5784.
99 D. W. Cho, M. Fujitsuka, U. Chan Yoon and T. Majima, *Phys. Chem. Chem. Phys.*, 2008, **10**, 4393–4399.
100 P. Xiao, W. Hong, Y. Li, F. Dumur, B. Graff, J. P. Fouassier, D. Gigmes and J. Lalevée, *Polym. Chem.*, 2014, **5**, 2293–2300.
101 F. Dumur, *Eur. Polym. J.*, 2022, **163**, 110962.
102 P. Majumdar, R. Nomula and J. Zhao, *J. Mater. Chem. C*, 2014, **2**, 5982–5997.
103 X. Xiao, W. Tian, M. Imran, H. Cao and J. Zhao, *Chem. Soc. Rev.*, 2021, **50**, 9686–9714.
104 X. Chen, A. A. Sukhanov, Y. Yan, D. Bese, C. Bese, J. Zhao, V. K. Voronkova, A. Barbon and H. G. Yaglioglu, *Angew. Chem., Int. Ed.*, 2022, e202203758.
105 A. Karimata, H. Kawauchi, S. Suzuki, M. Kozaki, N. Ikeda, K. Keyaki, K. Nozaki, K. Akiyama and K. Okada, *Chem. Lett.*, 2013, **42**, 794–796.
106 B. H. Drummond, N. Aizawa, Y. Zhang, W. K. Myers, Y. Xiong, M. W. Cooper, S. Barlow, Q. Gu, L. R. Weiss, A. J. Gillett, D. Credgington, Y.-J. Pu, S. R. Marder and E. W. Evans, *Nat. Commun.*, 2021, **12**, 4532.
107 X. Xiao, I. Kurganskii, P. Maity, J. Zhao, X. Jiang, O. F. Mohammed and M. Fedin, *Chem. Sci.*, 2022, **13**, 13426–13441.
108 S. Yamauchi and N. Hirota, *J. Chem. Phys.*, 1987, **86**, 5963–5970.
109 M. Terazima, S. Yamanuchi and N. Hirota, *J. Phys. Chem.*, 1985, **89**, 1220–1227.
110 M. Terazima, S. Yamauchi and N. Hirota, *Chem. Phys. Lett.*, 1985, **120**, 321–326.
111 M. Terazima, S. Yamauchi and N. Hirota, *J. Chem. Phys.*, 1986, **84**, 3679–3687.

